January 2017

Simulating Boundary Crossing Supercells Using A Non-Hydrostatic Cloud Model

Aaron Keith Scott

SIMULATING BOUNDARY CROSSING SUPERCELLS USING A NON-HYDROSTATIC CLOUD MODEL

by

Aaron K. Scott
Bachelor of Science, University of Oklahoma, 2013

A Thesis
Submitted to the Graduate Faculty

of the

University of North Dakota

In partial fulfillment of the requirements

for the degree of

Master of Science

Grand Forks, North Dakota
August
2017

This thesis, submitted by Aaron Scott in partial fulfillment of the requirements for the Degree of Master of Science from the University of North Dakota, has been read by the Faculty Advisory Committee under whom the work has been done and is hereby approved.

Chairperson

Committee Member

Committee Member

This thesis is being submitted by the appointed advisory committee as having met all of the requirements of the Graduate School at the University of North Dakota and is hereby approved.

Dean of the School of Graduate Studies

Date

PERMISSION

Title Simulating Boundary Crossing Supercells using a Non-Hydrostatic Cloud Model

Department Atmospheric Science

Degree Master of Science

In presenting this thesis in partial fulfillment of the requirements for a graduate degree from the University of North Dakota, I agree that the library of the University shall make it freely available for inspection. I further agree that permission for extensive copying for scholarly purposes may be granted by the professor why supervised my thesis work or, in his absence, by the chairperson of the department of the dean of the Graduate School. It is understood that any copying or publication or other use of the thesis or part thereof for financial gain shall not be allowed without my written permission. It is also understood that due recognition shall be given to me and to the University of North Dakota in any scholarly use which may be made of any material in my thesis.

Aaron Scott

8/1/2017

TABLE OF CONTENTS

LIST OF FIGURES

Figure Page

ACKNOWLEDGEMENTS

I would like to thank my advisor, Dr. Matthew Gilmore for his support and feedback throughout the course of this thesis project. I also thank Dr. Aaron Kennedy and Dr. Jianglong Zhang for their comments and suggestions during the project. I want to thank Ron Stenz for his help in code debugging and thoughtful comments. Finally, I thank my parents for all their love and support and for encouraging me to always pursue my dreams.

ABSTRACT

Supercell thunderstorms are among nature's most powerful phenomena. Particular environmental conditions are strongly correlated with peak supercell and tornado strength. However, supercells may experience changes within the near-storm environment during their lifecycle. For example, a storm may cross a preexisting outflow boundary from previous convection; thus, the storm will experience changes in the environmental thermodynamic and wind profiles. The purpose of this study is to determine what happens to the low-level mesocyclone immediately after crossing a boundary, analyze storm sensitivity to differing boundary crossing times, and show how the vorticity processes change as a storm moves from one environment to another.

An idealized cloud model is modified to simulate a heterogeneous environment in which there is a preexisting cold pool. A storm is initiated on the warm side of the boundary and crosses into the cool side. The low-level mesocyclone is analyzed as it crosses the boundary and Lagrangian trajectory analysis is performed to determine how vorticity is processed before and after crossing. This study finds that the low-level mesocyclone is cut-off as the preexisting boundary crosses the storm updraft; therefore, the low-level mesocyclone must reorganize on the cool side of the boundary. The environment on the cool side of the boundary is more conducive for low-level rotation but a stronger capping inversion may alter how vorticity is processed.

CHAPTER 1

INTRODUCTION

Supercell thunderstorms are one of nature's most powerful phenomena. Supercells are convective storms that have a quasi-steady rotating updraft and often last for more than two hours. Since they have long lifespans, they may encounter differences in wind and thermodynamic profiles over their lifetime. One such culprit for changes in the storm environment are preexisting outflow boundaries from previous convection. As a supercell encounters a boundary, changes in the storm morphology often occur and prior observational studies show that the storm becomes more likely to produce a tornado (Markowski et al 2001; Maddox et al 1980). However, most previous modeling work only used a homogeneous environment when investigating supercells (e.g., Weisman and Klemp 1982; 1984; Rotunno and Klemp 1985) or supercell tornadogenesis (e.g., Naylor and Gilmore 2012; 2014) and thus the specific importance of the boundary has not been addressed. The research proposed herein, will attempt to answer some outstanding questions related to why supercells and boundary interaction result in increases low-level rotation.

The following subsections will review previous literature on supercell storms, tornadic supercells in association with boundaries, and simulations of boundary-crossing storms. The review will define what a pre-existing boundary is within the context of this work. After a review, the research methods will be discussed in the methods chapter.

Convection

From an ingredients based approach, convective storms need three ingredients. Instability and moisture provide parcels the ability to rise within the atmosphere and condense into clouds, eventually forming rain. In order to realize the potential instability, the third ingredient, a lifting mechanism, is needed to provide a sort of push on parcels near the surface to rise within the atmosphere. It is common to observe such ingredients coexisting on a warm day in the spring and summer within the United States, but what distinguishes these basic convective storms from the storm cells that can last for several hours and produce severe weather?

In the 1950s and 1960s before the time of Doppler-radar, it was difficult to observe the wind field around such convective storms that seemed to last much longer than their lesser counterpart and appeared to deviate to the right of expected storm motion vectors. In 1964 Keith Browning termed the long-lasting, deviant storms the "Supercell" due to their enhanced lifetime. It was several years later scientists learned why supercells behaved in such a way.

The following sections discuss why and how supercell storms behave in such a way. It will follow with a review of how these supercell environments may change with time, as well as the implications these changes have on supercell behavior.

Supercell environments

It has been well established that supercell thunderstorms are among the most dangerous and hazardous storms in the United States. There are typical parameters that forecasters are trained to look for in pinpointing areas of supercell potential should a trigger mechanism be present for storms to form. High convective available potential energy

(CAPE), low convective inhibition (CIN), and sufficient vertical wind shear are recognized as the main ingredients for a supercell thunderstorm to flourish (Moller et al. 1994). The vertical wind shear can act to displace the storm updraft and downdraft, thus inhibiting rain drops from falling back into the updraft and causing downward momentum that acts to cut off the storm's inflow.

Weisman and Klemp (1982; 1984) were among the first to study the role of vertical wind shear and CAPE on idealized simulated supercells in homogeneous environments. These runs were deterministic in that the simulated storm was always the same, given a certain trigger magnitude and environmental conditions. In the model, these storms can last many hours. However, in real life, the storms can only last a long period of time under special conditions when storm remains isolated while moving through a quasi-homogeneous environment (Bunkers et al 2006).

Vertical wind shear generates horizontal vorticity that can then be tilted into the vertical as vertical vorticity by a storm updraft. The region of a storm that has strong tilting of horizontal vorticity into the vertical is called the mesocyclone.

In order to demonstrate how horizontal vorticity is tilted into the vertical, the vorticity tendency equations following Klemp and Rotunno (1983) are:

$$\frac{d\zeta}{dt} = \omega_H \cdot \nabla_H w + \zeta \frac{\partial w}{\partial z} + F_v, \quad (1)$$

$$\frac{d\omega_H}{dt} = \omega \cdot \nabla v_H + \nabla \times B\hat{k} + F_h, \quad (2)$$

where ω_H is the horizontal component of the vorticity vector, w is the vertical velocity, ω is the total vorticity vector, v_h is the horizontal velocity, B is buoyancy term, F_v and F_h are mixing terms. Equation (1) represents the vertical vorticity tendency and is influenced by the terms on the RHS, which are the tilting of horizontal vorticity and the stretching of

vertical vorticity, respectively. In (2), the first terms on the RHS represent the stretching of existing horizontal vorticity and the tilting of vertical vorticity into the horizontal and the second term represents horizontal vorticity via baroclinic production, respectively. Brandes (1984) showed that the mixing terms have little influence and can be omitted. Thus, in an atmosphere starting with no vertical vorticity, tilting of horizontal vorticity creates vertical vorticity. Figure 1 from Rotunno (1981) shows a unidirectional westerly vertical wind shear profile and how the horizontal vortex lines set-up along a north-south axis. As the updraft develops and inflow from the east flows into the updraft, the vortex lines are tilted into the vertical generating a cyclonic and anticyclonic vortex pair. Thus, this simple schematic illustrates how the tilting of horizontal vorticity acts to contribute to vertical vorticity.

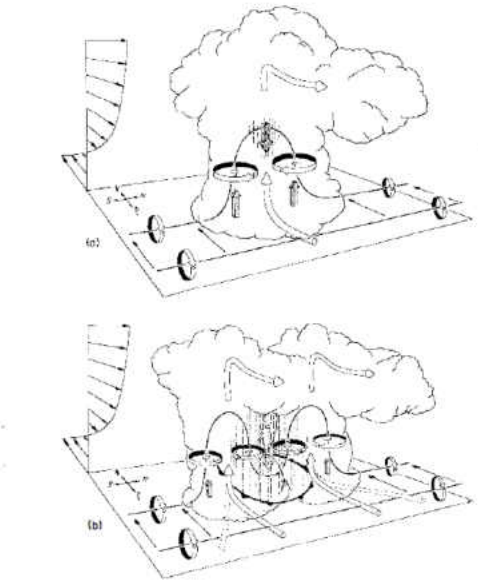

Figure 1. Schematic depicting how a typical vortex tube contained within (westerly) environmental shear is deformed as it interacts with a convective cell (views from the southeast). Cylindrical arrows show the direction of cloud-relative airflow, and heavy solid lines represent the forcing influences that promote new updraft and downdraft growth. Vertical dashed lines denote regions of precipitation. (a) Initial stage: Vortex tube loops into the vertical as it is swept into the updraft. (b) Splitting stage: Downdraft forming between the splitting updraft cells tilts vortex tubes downward, producing two vortex pairs. The barbed line at the surface marks the boundary of the cold air spreading out beneath the storm. (Taken from Rotunno 1981)

While the role of vertical wind shear on the formation of the mid-level mesocyclone is important, at lower levels, it has been shown that vertical wind shear is not sufficient and other mechanisms to produce such a low-level mesocyclone are at work (Rotunno and Klemp 1985). Baroclinically generated horizontal vorticity can be generated from a storm's induced outflow boundaries. Figure 2 shows a schematic by Lemon and Doswell (1979) of the forward and rear flank boundaries generated from the forward flank and rear flank downdrafts, respectively. Klemp (1987) offers a schematic of how parcels within the storm inflow may travel along the forward flank region and gain horizontal vorticity (Fig 3). Essentially, air parcels that travel along these outflow boundaries may gain enhanced horizontal vorticity due to the solenoidal effects induced by the rain-cooled air. This generation is accounted for in the second term in (2). It can be shown in a natural coordinate system, where $\vec{s}$ is along the boundary and $\vec{n}$ points toward the rain-cooled air, that streamwise horizontal vorticity is generated by

$$\frac{d\omega_s}{dt} = \frac{\partial B}{\partial n} \tag{3}$$

and B, buoyancy is,

$$B = g\frac{\Delta\theta_v}{\theta_v}. \tag{4}$$

where g is gravity, and θ_v is virtual potential temperature. Thus, as in Fig. 3, horizontal vortex lines are reoriented along the forward flank and parallel with inflow traveling along the forward flank; streamwise vorticity is created and ingested into the updraft where it is tilted into the vertical.

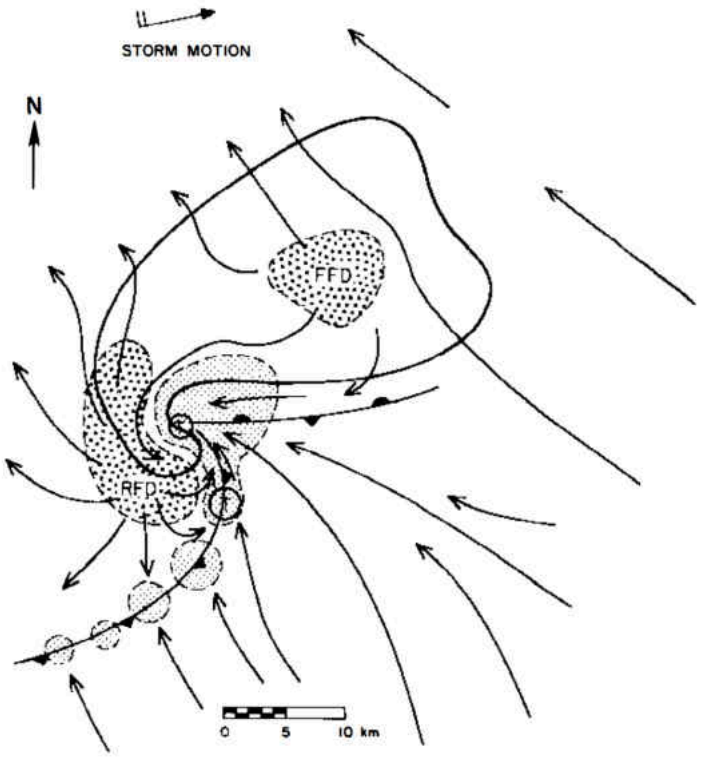

Figure 2. Schematic plan view of tornado thunderstorm near the surface. Thick line encompasses radar echo. The thunderstorm "gust front" structure and "occluded" wave are also depicted using a solid line and frontal symbol. Low-level positions of the updraft (UD) are finely stippled and forward flank downdraft (FFD) and rear flank downdraft (RFD) are coarsely stippled. Associated streamlines (relative to the ground) are also shown. Tornado location is shown by an encircled T. (Taken from Lemon and Doswell, 1987)

It has been shown that the augmentation of horizontal vorticity can be significant. For example, if a parcel has a residence time of 5 min within a 5°C thermal gradient, the parcel may obtain horizontal vorticity on the order of 6×10^{-5} s^{-2} (Rasmussen et al. 2000). However, there are multiple types of mesoscale boundaries that may aid horizontal vorticity production via the baroclinic mechanism. For example, anvil shadowing or outflow boundaries from other convection have been shown to produce horizontal vorticity along their edges (Markowski et al. 1998). It is these pre-existing outflow boundaries that are discussed extensively in the research herein.

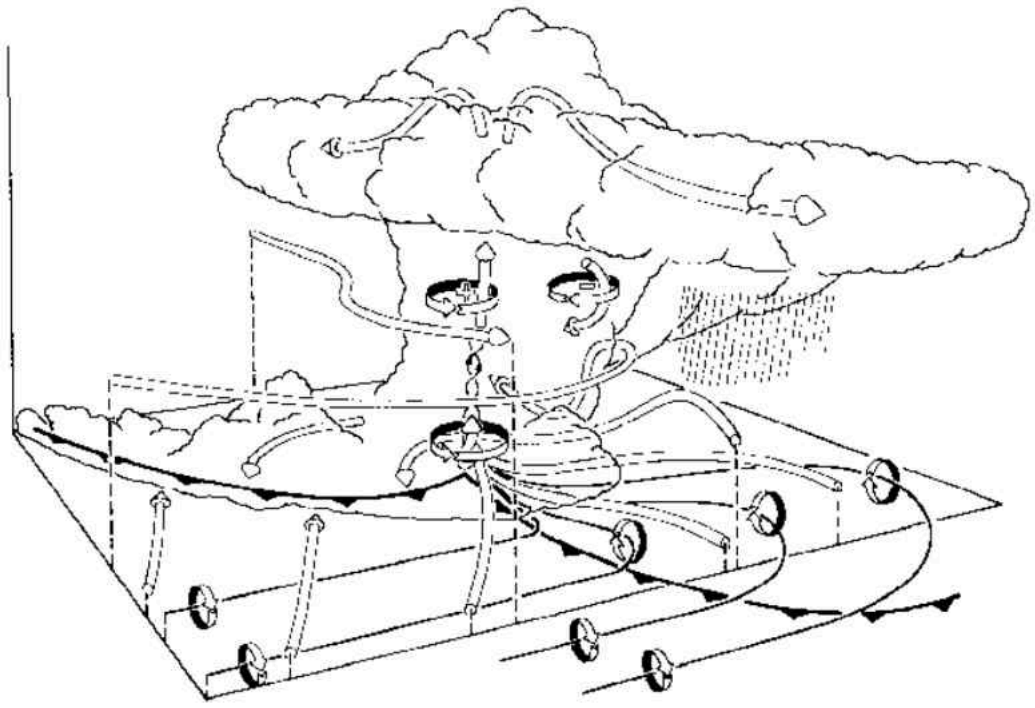

Figure 3. Three-dimensional schematic view of a numerically simulated supercell thunderstorm at a stage when the low-level rotation is intensifying. The storm is evolving in westerly environmental wind shear and is viewed from the southeast. The cylindrical arrows depict the flow in and around the storm. The thick lines show the low-level vortex lines, with the sense of rotation indicated by the circular-ribbon arrows. The heavy barbed line marks the boundary of the cold air beneath the storm. (Taken from Klemp 1987)

Tornadic supercell environments

While key ingredients are needed within supercell environments, it has already been stated that not all supercells produce tornadoes. Several efforts have been made to elucidate environmental factors that may differentiate environments of tornadic and non-tornadic supercells. Thompson et al. (2003), hereafter T03, used proximity RUC soundings from observed supercell storms that were categorized as significantly tornadic to non-tornadic. Their findings revealed that 0-1 km SRH (storm relative helicity) and MLLCL (mixed layer liquid condensation level) height did the best at distinguishing between the tornadic and non-tornadic supercell classes. Over 80% of significantly tornadic storms were in environments categorized with relative humidity > than 65% and 0-1 km SRH > 75 m^2s^{-2}.

TO3 developed the Significant Tornado Parameter (STP) to help forecasters use the various parameters in unison. The STP is defined as

$$STP = \left(\frac{MLCAPE}{1000}\ J\ kg\right)\left(\frac{SHR6}{20}\ ms^{-1}\right)\left(\frac{SRH1}{100}\ m^2 s^{-2}\right)\left[\frac{2000-MLLCL}{1500} m\right] \quad (5)$$

where SHR6 is the vector shear magnitude from 0-6 km AGL, SRH1 is storm relative helicity from 0-1 km, MLCAPE and MLLCL have the standard definitions. Equation 5, is formed such that TO3 developed the thresholds based upon their distributions derived from the proximity soundings that show skill discriminating between significantly tornado and non-tornadic. For example, no cloud bases were over 1750 m for the significant tornado cases; therefore, STP goes toward zero when MLLCL height approaches 2000. Likewise, if MLCAPE or SRH go toward zero, then STP approaches zero. These parameters reiterate what is thought to be important for a tornado environment: high cape, streamwise helicity, and low cloud bases.

Naylor and Gilmore (2012), hereafter NG12, used the significantly tornadic close-proximity soundings from T03 to simulate tornadoes within an idealized cloud model to study tornado longevity and strength. From their study, 21 of the soundings produced simulated tornadoes and revealed a near linear relationship between 0-3 km SREH and tornado longevity. In addition, 0-1 km SREH was a close linear fit. Other parameters like CAPE and LFC height did not have a strong correlation when used alone; however, when used in a multiple linear regression, CAPE, Pwat, and LFC height did a decent job.

From the above studies, it can be inferred that SREH in the lower levels likely plays a key role in tornado production and longevity. However, what are some mechanisms for SREH and how could it change over time? NG12 stated several potential caveats in their study with one of those being the horizontally homogeneous nature of the model

environment. Changes within the environment occur as the storm progresses in both time and space. As has been shown in other studies, SREH can be changed via storm-induced effects (citations here), but also there are environmental changes a storm may encounter that could alter the production or advection of SREH. In the study herein, changes in SREH and thermodynamics are studied from influences of a boundary.

Previous work on supercells interacting with boundaries

Observations. As early as the 1950s, scientists noted the association between preexisting boundaries and supercell tornadoes (e.g., Kuhn et al. 1958; Magor 1959; Miller 1967). These early works noted the importance of recognizing thermal boundaries and their implications on tornado forecasting. Maddox et al. (1980) documented numerous tornadic supercells that were associated with thermal boundaries. Based upon those cases, they offered a conceptual model for the intensification of supercells and increased tornado likelihood as they moved across and along baroclinic boundaries (Fig 4). They discussed how variations in thermal gradients could alter the winds in the boundary-layer. These alterations were then argued to lead to moisture convergence and vertical vorticity enhancement along a narrow axis of a low-level thermal boundary. Maddox et al. (1980) documented that if a storm crossed a boundary, it produced short-lived but intense tornadoes, while storms propagating along boundaries produced long-lived and sometimes violent tornadoes.

Satellite data has shown several storm and boundary interactions within the United States (e.g., Weaver and Nelson 1982; Purdom 1993; Weaver et al. 1994). Weaver and Purdom (1995) used a series of satellite images to show an interaction between a supercell and a preexisting boundary. In proximity to this boundary, the storm produced a series of

tornadoes including a damaging F5 in Kansas. While many of these satellite studies appear to show changes in storm morphology as it crosses a boundary, these data sets do no provide the ability to quantitatively show how a storm changes with respect to low-level rotation, updraft strength, or other parameters.

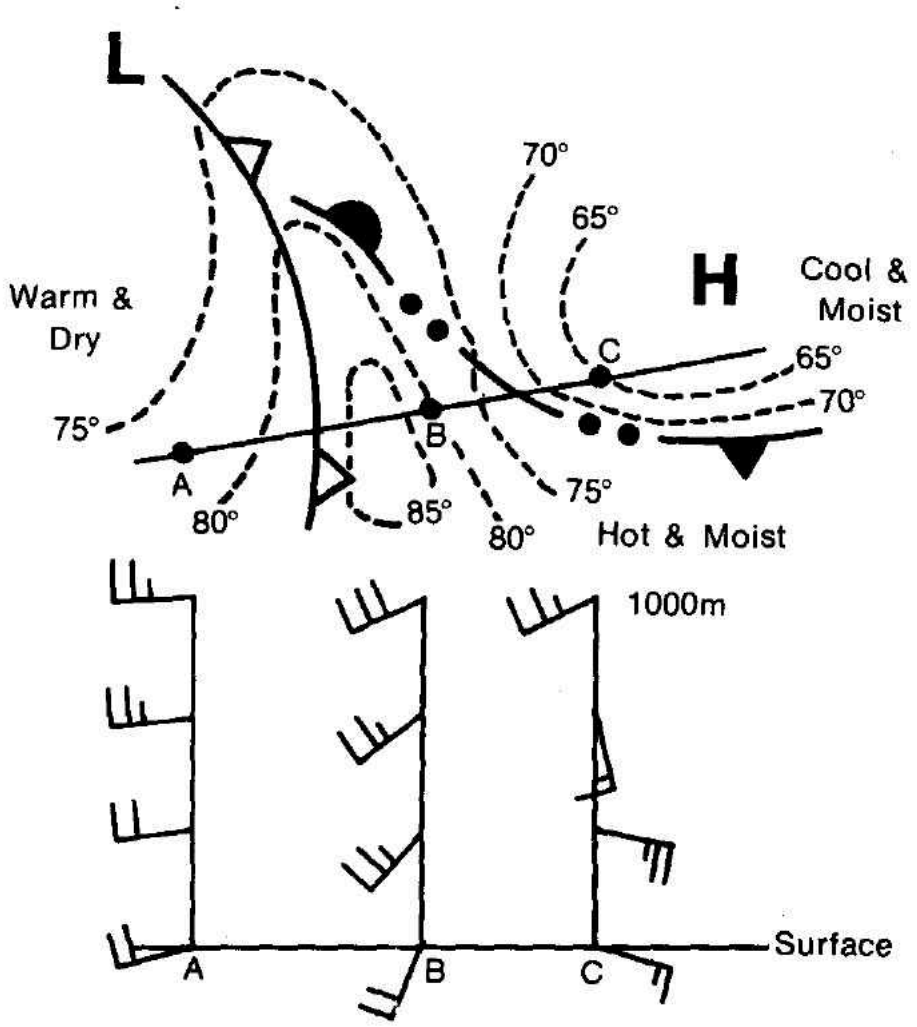

Figure 4. Schematic representation of boundary-layer wind profiles within a typical severe-thunderstorm-producing surface pattern. (From Maddox et al. 1980)

In the mid-90s, the NSF-funded field campaign, Verification of the Origins of Rotation in Tornadoes Experiment (VORTEX - Rasmussen et al. 1994), was used to document the environments near supercells along with high-resolution mobile radar

observations and detailed mobile-mesonet observations that could be used to measure conditions across boundaries. This project led to several published case studies. One of the most remarkable findings was that close to 70% of the significant tornadoes during the experiment occurred near low-level preexisting boundaries (Markowski et al. 1998) and thus the boundaries appeared to provide a means for increasing storm rotation. Markowski et al. (1998) suggests that tornadogenesis requires augmentation of the horizontal vorticity produced by the environmental wind shear via boundaries. Only in instances where the deep layer shear is over 50 ms^{-1} can the forward flank baroclinic effects provide additional vorticity needed for tornadogenesis. In cases were the shear is lower, a preexisting boundary unrelated to the storm itself is needed to augment the vorticity since residence times of parcels along the boundary are longer than residence times of parcels traveling along the forward flank. While these findings are important, the evidence of boundary importance on vorticity production in VORTEX is a small sample size. However, these results did seem to support prior research associating preexisting boundaries with increases in storm rotation, longevity, and most importantly tornadogenesis.

Blanchard (2008) presented a case from VORTEX previously undocumented by Markowski et al. (1998) of a supercell thunderstorm manipulating an outflow boundary. This storm drew the outflow boundary northward into the storm's inflow region. The storm then appeared to gain strong low-level rotation as the boundary was drawn northward into the updraft region. Despite the interaction with the boundary and enhanced low-level rotation, this storm did not produce a tornado.

The environment nearby and along a preexisting outflow boundary from 2 June 1995 has been studied extensively (e.g., Rasmussen et al. 2000; Gilmore and Wicker 2002).

The environment immediately along and into the cool side of the boundary was characterized as having higher CAPE, boundary-layer moisture, and low-level vertical shear. These observations, when related back to the STP, yield an increased potential for tornadoes on the immediate cool side of the boundary. The observations and modeling simulations from this case, as will be discussed in the next section show a steady increase in storm strength. This coincides with an observed increase in tornado production following the boundary crossing.

Modeling. Idealized modeling studies, such as that of Klemp and Rotunno (1983), have shown that horizontal vorticity can be produced within the baroclinic zone produced by evaporatively-cooled outflow from a supercell's downdraft region. This low-level horizontal vorticity is produced due to solenoidal effects from horizontal gradients (i.e., temperature changes across the boundary). Furthermore, both modeling and observational studies have shown that strong horizontal vorticity production can occur along these baroclinic boundaries (Rotunno et al. 1988; Rasmussen and Rutledge 1993). The modeling study of Brooks et al. (1993) showed that the large accelerations in storm inflow could lead to stretching of the baroclinically-enhanced horizontal vorticity before tilting into the vertical by the storm's updraft.

Atkins et al. (1999) conducted a case study on a storm/boundary interaction using a non-hydrostatic cloud model. By simulating a homogeneous and non-homogeneous case, they found that the low-level mesocyclone formed much earlier, was stronger, and lasted for a longer period when a boundary was present. They also noted that boundary orientation with respect to storm motion was a key factor in the low-level mesocyclone evolution. It was found that storms moving along a boundary or moving into the warm

side had stronger mesocyclones. Moreover, Atkins et al. (1999) used backward trajectories from the mesocyclone to track the source regions of the air coming into the mesocyclone. It was found that the forward flank was crucial in generating vorticity as parcels traveled along it in the no-boundary case. The boundary case showed more parcels came from behind the boundary and from the storm inflow at low-levels with only 11% of the parcels originating from the forward flank. This case also demonstrated that parcels in the low-level mesocyclone came from the mid-levels while the no-boundary case had approximately 30% of the parcels originating from the mid-levels and traveling along the forward flank. This suggests that the mechanism for which low-level vorticity is acquired is much different for storms in the boundary and no-boundary cases. These analyses will be furthered in the study herein.

Storms do not always experience such drastic horizontal changes in their environments. Richardson et al. (2007) studied the evolution of storms in a slowly varying environment. By altering the vertical shear slowly over a section of the domain, storm morphology changed as the storm encountered the changing environment. Davenport and Parker (2015) used a technique called base-state replacement (Letkewicz et al. 2013) to simulate the environment of a decaying supercell from the VORTEX2 campaign. They found that the decrease in buoyancy had the most significant impact on storm demise rather than the vertical wind shear. Both of these studies continue to demonstrate that storm vitals are greatly impacted by changing environments and have highlighted the fact that an environment a storm forms in very well may not be the same environment in which a storm dissipates.

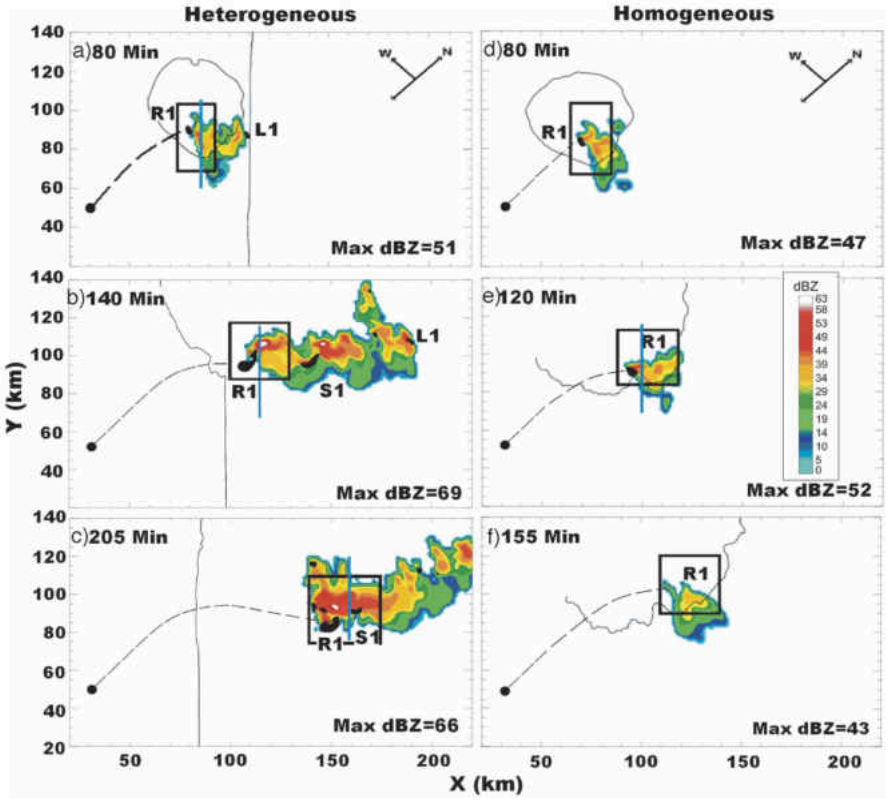

Figure 5. Simulated radar reflectivity calculated using the Ferrier (1994) technique at z = 1.5 km plotted in a ground-relative reference frame for the heterogeneous environment (a) before storm R1 crosses the boundary (t = 80 min), (b) after R1 crosses the boundary corresponding to (d) the same time as in (a) (t = 80 min), (e) during storm R1's most intense updraft phase (t = 120 min), and (f) as R1 dissipates (t = 155 min). The black-filled contours represent updraft speeds greater than 15 m s^{-1} at z = 4.6 km. The think black lines are the surface potential temperature perturbation of –1 K relative to the initialization sounding on the warm side of the boundary. Note that the domain is skewed relative to the compass shown in (a) and (d). (Taken from Fierro et al. 2006)

While these slow changes may happen often, rapid changes induced by outflow boundaries can be of societal significance since they could change storm morphology quickly. Fierro et al. (2006) used two soundings from the 2 June 1995 outflow boundary case of VORTEX and modeled the effects of the outflow boundary on a mature simulated supercell to study electrification and lightning. The storm is initialized on the warm side and crosses the low-level boundary into a cooler environment; however, the environment immediately behind the boundary was characterized by having higher CAPE, boundary layer moisture, and low-level vertical wind shear (Gilmore and Wicker 2002). Figure 5 shows horizontal cross sections of simulated reflectivity from a heterogeneous (boundary

crossing) and a homogenous (single air mass) simulation. Notice the right moving storm dissipates in the homogenous case but appears to increase in strength when it crosses the boundary in the heterogeneous simulation. Indeed the storm was found to increase in vitals such as updraft speed, 40-dBZ echo-top, and low-level mesocyclone rotation as it crossed the boundary (Fig. 6). There was an increase in graupel and hail volumes, which may have played a factor in the increase in more frequent cloud-to-ground lightning flashes. While the study herein does not aim to study electrification, the individual contributions from vertical wind shear, CAPE, and boundary-layer moisture are of interest in unveiling what factor contributed most to the storms increase. It would be of interest to note whether the individual contributions stated above would differ in importance from Davenport and Parker (2015). Fierro et al. (2006) found considerable resemblances to the storm behavior in nature and is the foundation for which the study herein bases its methodology.

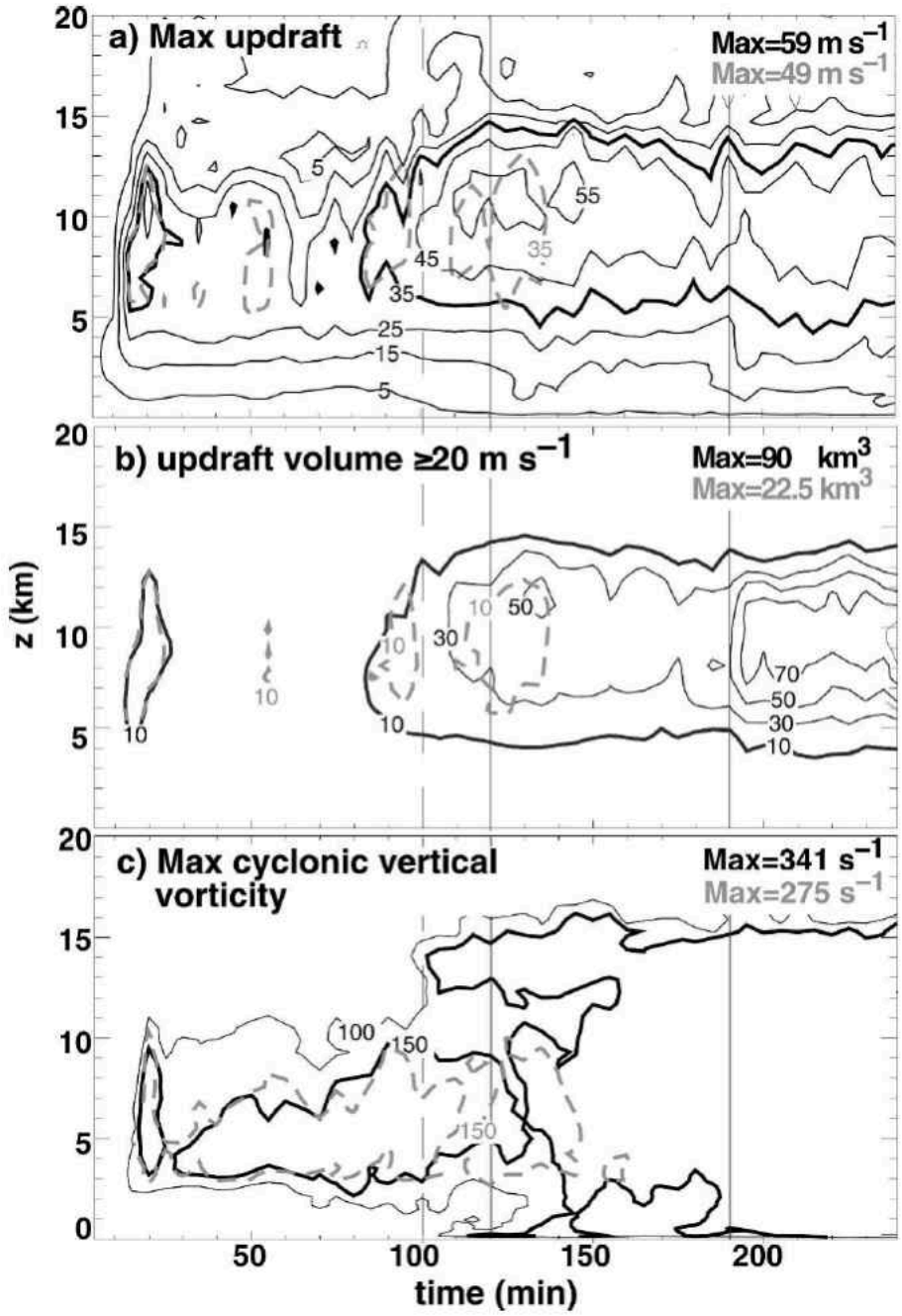

Figure 6. Time-height contour plots of (a) maximum vertical updraft speed (m s^{-1}), (b) updraft volume greater than 20 m s^{-1} (km^3), and (c) maximum cyclonic vertical vorticity (1x10^4 s^{-1}) within a box following storm R1 for the heterogeneous environment (black) and homogeneous environment (gray dashed). In all plots, the solid vertical line (t = 120 min) indicates the time when the R1 storm crosses the boundary and the dashed line just prior (t = 100 min) shows the time when the storm starts to experience the new environment. Extrema for the time series are shown in the upper right corner. (From Fierro et al. 2006)

CHAPTER 2

METHODOLOGY

Initial Conditions

In the early morning hours of 2 June 1995, a complex of thunderstorms was in progress across the Texas panhandle and western Oklahoma. As the complex moved to the east, rain cooled air created a low-level cold pool that spread out from the storm complex (Gilmore and Wicker 2002). The leading edge of the cooler denser air mass was the focus of new storm development as well as tornadic activity as storms crossed the boundary. Figure 7 shows the outflow boundary propagating outward from the storm complex as observed from satellite.

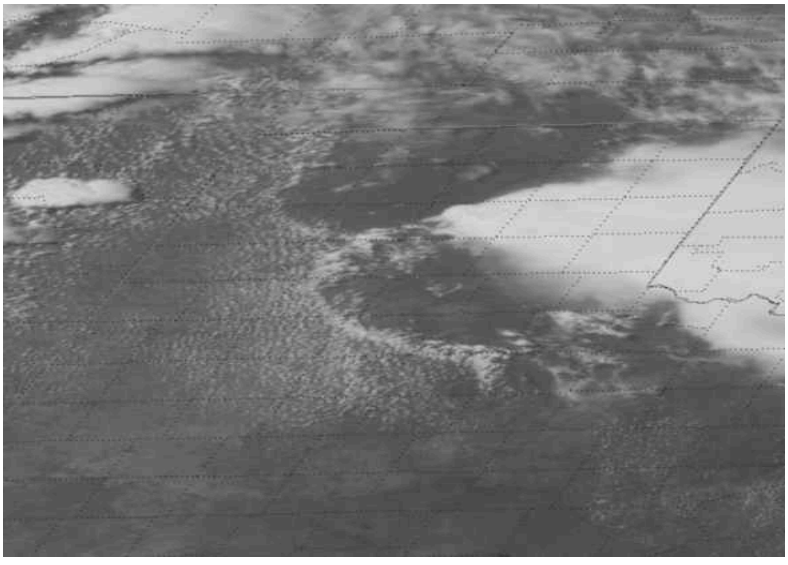

Figure 7. Visible satellite image from 2 June 1995 showing the preexisting boundary in the Texas Panhandle. The white mass on the right is an on-going MCS that produced the preexisting boundary from the MCS outflow.

Atmospheric soundings and mobile mesonet sampled the atmosphere during the VORTEX-95 field campaign on 2 June 1995 in the Texas panhandle near the outflow

boundary (Rasmussen et al. 1994; Gilmore and Wicker 2002). These soundings, and mobile mesonet transects, retrieved conditions on both sides of the outflow boundary. The two soundings used to initialize the boundary in the research herein come from Fierro et al. (2006), hereafter Fierro06, which are based upon work done by Gilmore et al. (2002), hereafter Gilmore02.

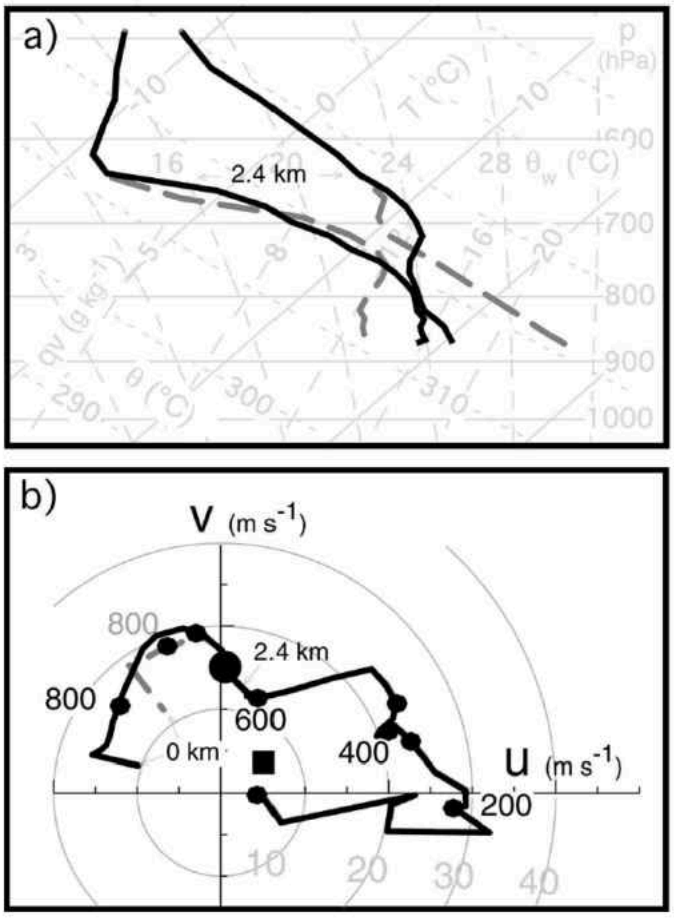

Figure 8. (a) Skew T-log P diagram and (b) hodographs used to define the initial conditions on the warm (gray dashed line) and cool (black line) sides of the boundary. Both hodographs are soundings used in the initialization are identical to the Hub, TX, sounding above z = 2.4 km AGL. Hodograph pressure levels are indicated with black dots every 100 hPa and are labeled every 200 hPa. (Adapted from Fierro et al. 2006)

Figure 8 shows both soundings overlaid. Sounding 1 (called "warm side sounding", hereafter) sampled the warm environment ahead of the outflow boundary. Fierro06 discussed the modifications made to both soundings, also summarized herein. The warm

side is a composite of the 2058 UTC Hub, Texas and the 2315 UTC Lubbock, Texas soundings. The Hub, TX thermodynamic profile is used while the winds were replaced with data from Lubbock, TX below 1.9 km AGL. This combination is used since the Hub, TX thermodynamic profile and Lubbock, TX low-level wind profile were found by Gilmore02 to be most conducive for storm development and longevity in the warm side environment. The second sounding (called "cool side sounding", hereafter) was launched on the immediate cool side of the boundary near Lockney, Texas. Since the model does not have terrain, the surface pressure was adjusted to match the warm side (Gilmore02). Fierro06 additionally modified the temperature at the top of the boundary layer to increase CIN and suppress secondary cell development on the cool side to minimize other storm interaction with the main storm being studied.

In nature, storms that either remained on the warm side of the boundary, crossed the boundary, or formed on the boundary. To study why warm side storms crossing the boundary were observed to produce stronger low-level mesocyclones, compared to storms that remained in the single air mass, two different model configurations are used herein. Homogenous (warm side sounding only) and heterogeneous (warm and cool side soundings) runs are conducted to analyze differences in storm morphology and low-level rotation characteristics. The following section describes the model configuration and initialization.

Model Set-up

Heterogeneous Simulations

The three-dimensional cloud model, CM1 (Bryan and Fritsch 2002), is used for simulations herein. CM1 is a fully compressible non-hydrostatic cloud model from NCAR

(National Center for Atmospheric Research) that has been used in the literature for over 15 years in convective modeling studies (Bryan et al. 2003). A model domain of (x,y,z) = (228 x 168 x 20) km is used with 500 m horizontal and 100 m vertical grid spacing. The simulations are run for 10000 s with history files saved at 100 s intervals. Restart files are saved every 2000 s in order to rerun certain times of the model to output 5 s history files for further analysis. The time-split method is used for time stepping as has been historically used (Klemp and Wilhelmson 1978a). The large time step is 1 s and the small time step is set to 0.167 s. Coriolis and friction forces are turned off in the model. A Rayleigh damper is applied above 16 km to reduce the impacts of gravity wave reflection. The lateral boundary conditions are gravity wave radiating and lateral Rayleigh damping is turned off since the preexisting outflow boundary is in contact with the lateral edges of the model. This is an issue since the lateral boundary conditions will retain whatever value of theta (and other variables) that touches them, thus causing the outflow boundary to become oriented off axis. Morrison microphysics is used for all simulations.

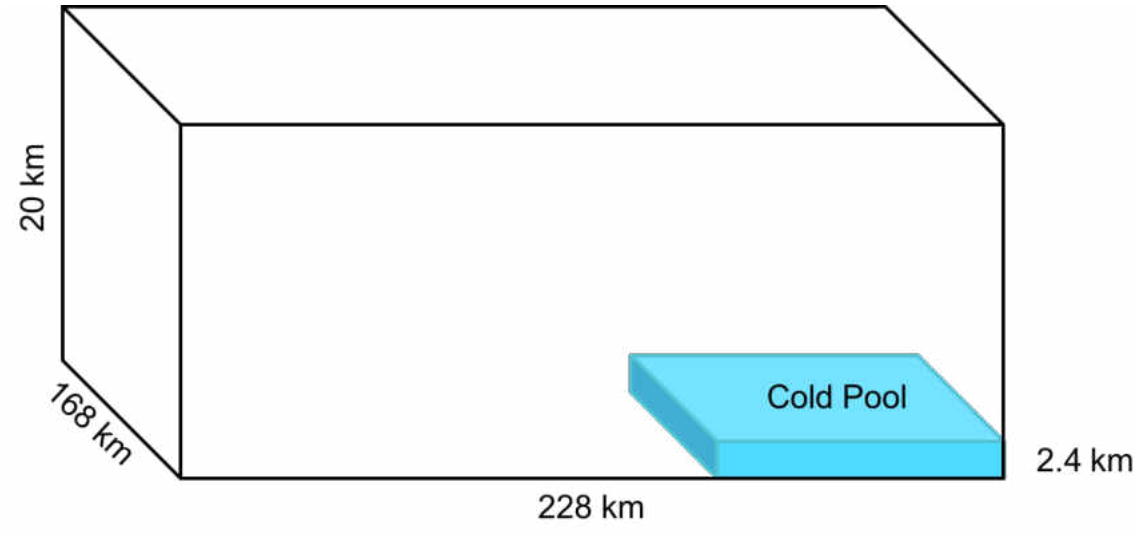

Figure 9. Schematic 3D view of the model domain at initial model time. The numbers represent length, width, and height of the model, respectively. 2.4 km represents the height of the cold pool at the initial model time. As the model integrates forward in time, the cold pool propagates toward the left side of the domain.

While most researchers that utilized cloud models perform simulations with homogeneous initial conditions (i.e., one thermodynamic and wind profile), the initialization of an environment similar to that with an outflow boundary requires a different technique. The methodology of Fierro06 is followed, where two soundings are used in the initialization of the model: a warm side and cool side sounding. Above 2.4 km, the warm side is used everywhere within the domain; as outflow boundaries are low-level features, only the lowest 2.4 km contains the variation (Fig 9). A hyperbolic tangent function is used to vary between the two soundings in a narrow region in the model domain. This function is used for mathematical convenience and not because it reproduces the detailed structure of a density gradient. The model must run approximately 15 minutes before a more realistic density gradient appears (such as what is shown in Droegemeier and Wilhelmson 1987). The boundary is initialized so that the average of the two soundings is at approximately 2/3 of the way across the domain with a transition zone of 14 km. Away from the transition, the left side contains the warm sounding and right side the cool side sounding. Figure 10, shows the surface theta variation at model initialization time.

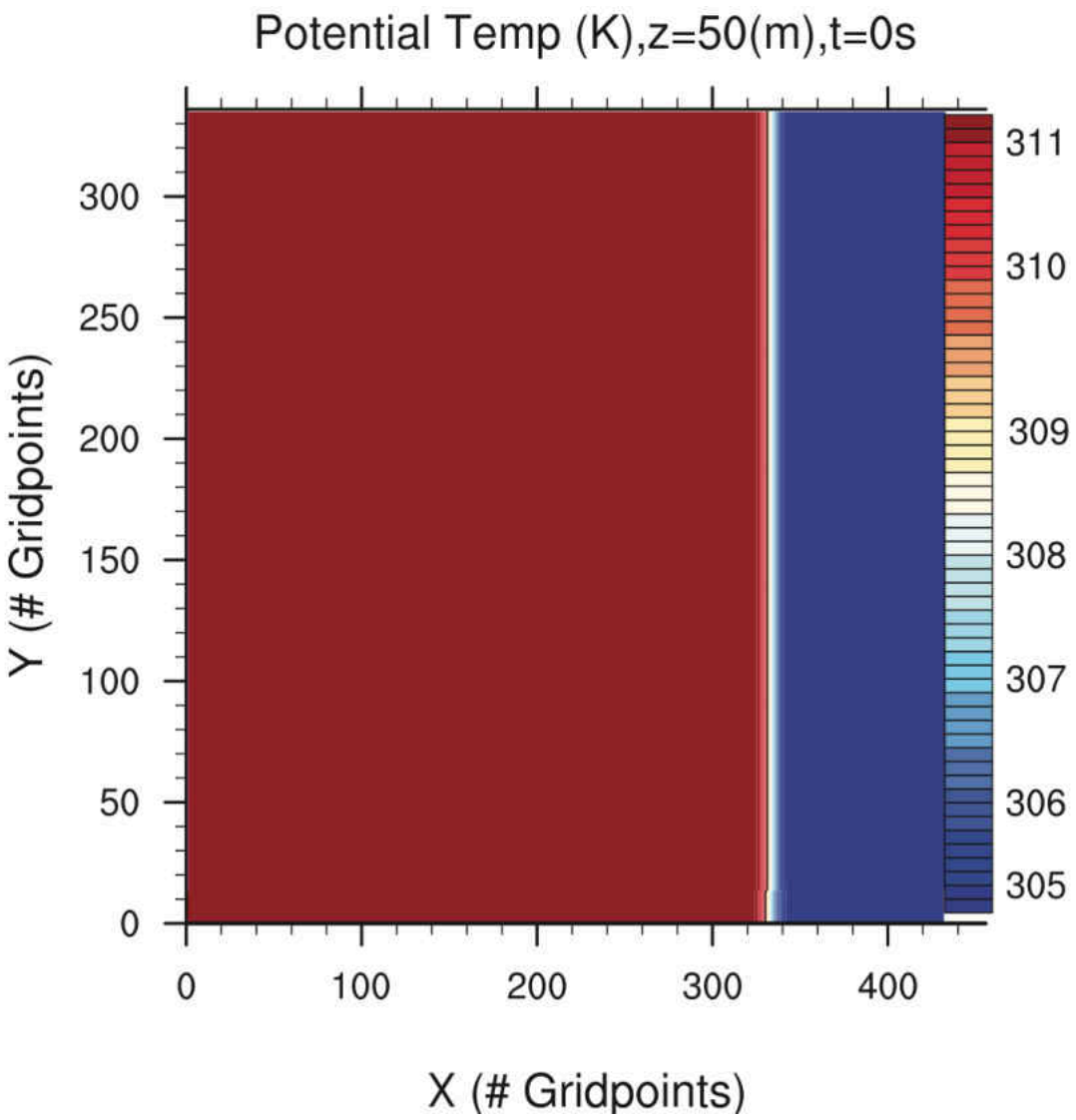

Figure 10. Plan view of potential temperature (K) at the lowest model level (z = 50 m) at model initialization time.

In nature, the boundary was curved from nearly N-S in the northwest Texas Panhandle to NW-SE in the Central Texas Panhandle. Two of the best-studied boundary crossing storms from that day occurred near Friona and Dimmitt, TX, where the boundary was oriented from northwest to southeast. Thus, that orientation is of most interest here. In the model, for convenience and to avoid numerical artifacts, the boundary is implemented such that it is parallel to the domain's y-axis. The wind profiles are rotated clockwise 45° so that the model boundary is effectively NW-SE. In essence, a coordinate

transformation has occurred. Thus, north points toward the upper right corner of the model domain for all heterogeneous simulations (Fig 11).

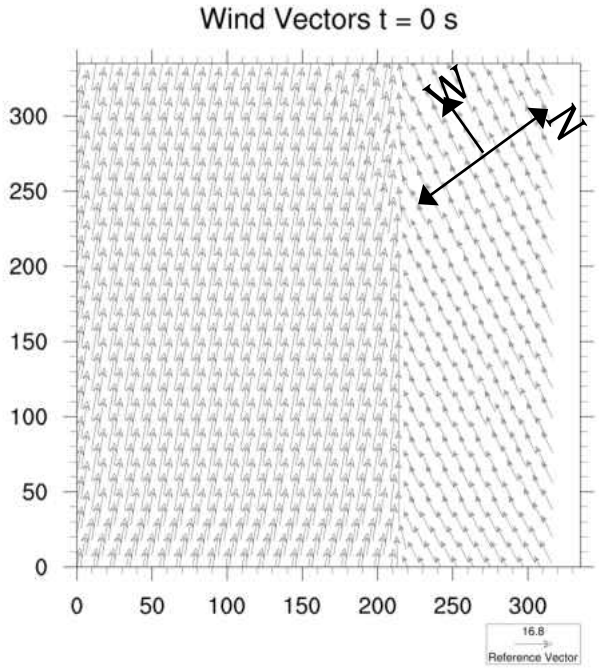

Figure 11. Same as fig. 10 except for wind vectors. The boundary is parallel to the domain's y-axis. The winds are shifted so they are similar relative to the observed boundary. The compass indicates the rotated reference.

Storms are initiated with a common technique first developed by Klemp and Wilhelmson (1978). An axisymmetric warm bubble with a maximum temperature perturbation of 3 K centered 1.5 km AGL and horizontal and vertical radii of 10 and 1.5 km, respectively, is placed on the warm side of the boundary. The starting point of the boundary (–1 K theta perturbation line) and the warm bubble are placed within the domain so that the storm will be mature when the boundary and storm approach one another. In the model, a moving grid is employed to keep the storm in the center of the domain at maturity (following KW78). Thus, the boundary will appear to move toward the left (SW) faster than it would if the grid was stationary.

Homogenous Runs

In order to determine if the boundary had an impact on the storm's overall characteristics as compared to a storm in a more homogenous environment, one homogenous run was completed. As is common practice, a single sounding is used to initialize these runs. The warm side sounding is initialized at all points and a 3K warm bubble is used to start convection. Although there is no physical reason to rotate the winds in these simulations, the winds will be rotated simply to make comparing storm motion to the boundary simulation storms easier. All other model settings are the same as the heterogeneous simulations except horizontal damping is switched on. The homogenous run will be identified as the WarmRun, hereafter.

Sensitivities

To study the sensitivity of boundary crossing time on storm morphology, storms are initiated at varying distances from the boundary at the initial model time. This is done by placing the warm bubble at different distances from the boundary (Fig 12). These variations cause the storm and boundary to interact at different times within the storm lifecycle. For example, a storm initiated by placing the warm bubble at 96 km from the boundary should be more developed than a storm initiated closer to the boundary. For this study, five experiments are performed varying the warm bubble from the boundary initially at 54, 73, 92, 111, and 130 km apart.

In an attempt to save computational time, earlier attempts of the simulations herein employed a smaller model domain than is shown within the results section. In doing the storm maturity sensitivity tests, the right moving storm 96 km simulation did not survive before crossing the boundary. Since Fierro06 initially had a distance of 100 km between

the warm bubble and boundary, using a larger domain, the same domain from Fierro06 was adopted for use.

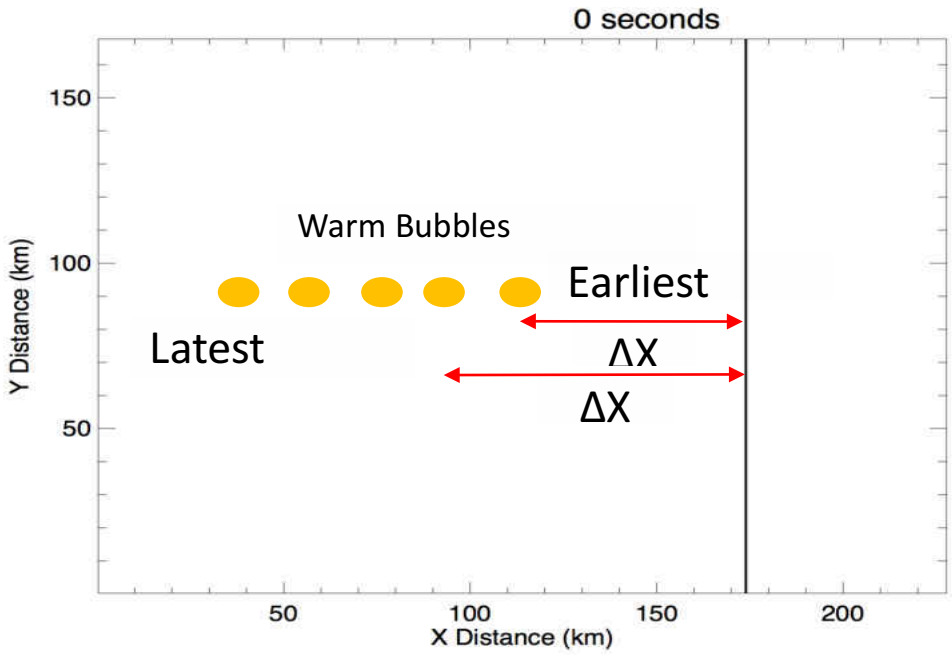

Figure 12. Schematic illustrating the storm initiation (indicated by the yellow ovals) location relative to the boundary (ΔX). The solid black line is the location of the boundary at t = 0. The yellow oval closest to the boundary crosses the boundary at the earliest time and the yellow oval to the far left crosses the boundary at the latest time.

Analysis

The analysis focuses on understanding what changes occur within the storm as it crosses into the new environment. The goal of the initial analysis is to show that changes in storm strength and characteristics are impacted by the boundary and new environment. Detailed analysis of the circulation budget and parcel source regions are studied with the use of circulation and trajectory analysis techniques. The goal of these analyses is to elucidate changes to the circulation around the storm's updraft and note changes to source regions for parcels that are being ingested into the

mesocyclone. It is also shown how parcels are influenced by the various mechanisms that generate vertical vorticity. Details and goals on each of the analysis techniques are discussed in the remainder of this chapter.

General Analysis

Horizontal cross sections of simulated reflectivity with the -1 K theta perturbation overlaid are used to provide times for when the storm and boundary interactions occur. Time-height plots are created to illustrate the changes in reflectivity, updraft speed, updraft volume, and vorticity before, during, and after boundary crossing time. In order to ensure that data used in the time-height plots are representative of the storm in question, since other convection develops in the model, an analysis box is centered over the maximum updraft helicity and is made large enough as to ensure the entire updraft of the storm is within the box. The maximum value of each variable is extracted at each height within the analysis box to create the time-height plots.

Trajectory Analysis

The use of backward trajectories allows for a study of the vorticity properties that parcels possess entering the mesocyclone, before, during and after boundary interaction. This analysis also provides insight, about the paths parcels take on their journey to help elucidate how vorticity is acquired. A backward trajectory analysis technique is applied and this follows a similar approach from Naylor and Gilmore (2014). Minor revisions to this technique are made to account differences in spatial resolution. In summary, trajectories are seeded within a 4km x 4km x 0.5km box around the low-level mesocyclone. The analysis box is centered over the UH

maximum. For mesocyclones, grid points must exceed a vertical vorticity threshold of 0.01 S^{-1} to ensure they are within the main circulation. Due to computational constraints, a maximum of 100 trajectories are allowed within the analysis at a given time. The trajectories are stepped backward in time every 5 s until 900 s back in time is reached. It has been shown that 5 s temporal resolution is sufficient for accurately tracking trajectories and 900 s is adequate for discovering the parcel source regions (Dahl et al. 2012). Since it is of interested in how parcel source regions and vorticity production acting on parcels may change with the interaction of a boundary, trajectories will be placed in the low-level circulation three separate times. These times will be selected to study trajectories before, during, and after the storm crosses the boundary.

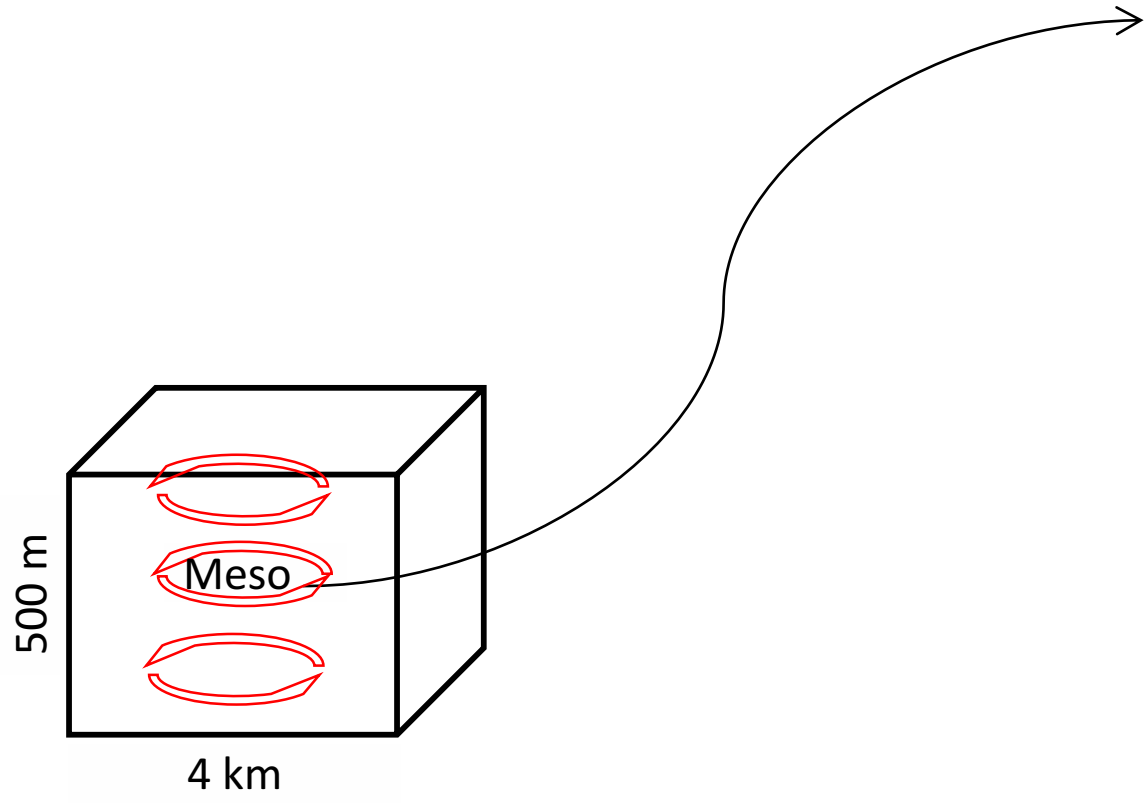

Figure 13. Schematic illustrating the analysis box in which trajectories were released within the mesocyclone. The x and y – axes are 4 km and the z-axis is 500 m. The red circular patterns represent the mesocyclone at various vertical levels in the lowest 500 m. the black line coming out of the box represents a simplified example of a trajectory being tracked backwards in time from its location in the mesocyclone.

The parcel positions are tracked by using a fourth-order multistep Runge-Kutta method. At each time step, trilinear interpolation from the surrounding eight grid points is used to calculate scalar and wind vector information of the parcel. To track vorticity tendencies along the trajectory path, first-order discretization of:

$$\frac{d\zeta}{dt} = \omega_H \cdot \nabla_H w + \zeta \frac{\partial w}{\partial z}, \qquad (4)$$

$$\frac{d\omega_H}{dt} = \omega \cdot \nabla v_H + \nabla \times B\hat{k}, \qquad (5)$$

where ω_H is the horizontal component of the vorticity vector, w is the vertical velocity, ω is the total vorticity vector, v_h is the horizontal velocity, and B is buoyancy term, are calculated following Klemp and Rotunno (1983). Equation (4) represents

the vertical vorticity tendency and is influenced by the terms on the RHS, which are the tilting of horizontal vorticity and the stretching of vertical vorticity, respectively. In (5), the first terms on the RHS represent the stretching of existing horizontal vorticity and the tilting of vertical vorticity into the horizontal and the second term represents the horizontal production of horizontal vorticity due to baroclinic effects.

The trajectories are separated into descending and ascending categories. A trajectory is said to be descending if it started from a height of at least 1 km and descended toward the surface. Ascending trajectories start near the surface and traveled along the forward-flank gust front and rose towards the tornado or mesocyclone.

CHAPTER 3

RESULTS AND DISCUSSION

Storm Morphology – Control Run

In this section, storm morphology is shown and discussed for the control run. The morphology is described from both a ground-relative (absolute time) perspective and a boundary-crossing-relative perspective. Herein, time, *t*, is measured from the beginning of the simulation and Δt represents time relative to the updraft's boundary crossing; thus, $\Delta t=0$ is time of boundary crossing and $\Delta t= -10$ min is 10 minutes before the storm updraft crossed the boundary. The boundary crossing time is defined as the point when the low-level updraft contour first crosses the –1 K warm base state perturbation potential temperature contour associated with the pre-existing boundary at the model surface. This near-ground "surface" is defined as the lowest model scalar grid level (z = 50 m). The reader is reminded that the term boundary, explicitly means the pre-existing outflow boundary, unless otherwise stated.

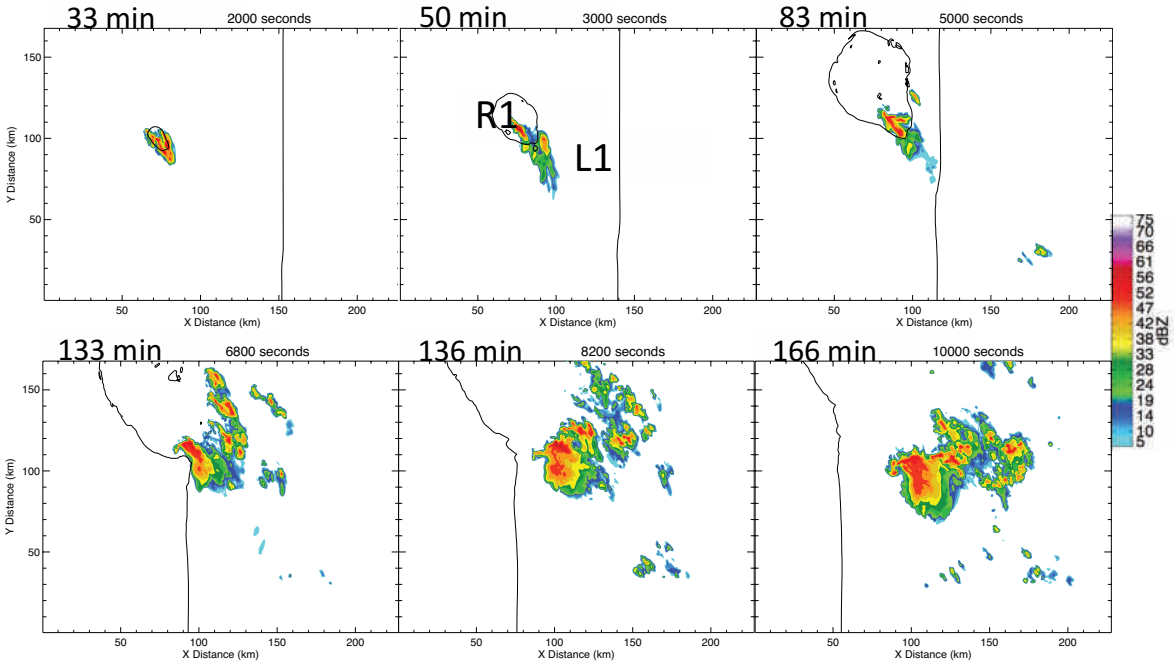

Figure 14. Simulated reflectivity horizontal cross sections at z = 1.5 km. The black contours denote the –1 K surface theta perturbation from the warm side base state sounding.

Figure 14 shows the evolution of the simulated storm. The initial storm started to split into right- and left-moving supercells (R1 and L1, respectively) at 33 min and L1 dissipated between 50 and 70 min (not shown). During the split, maximum updraft values temporarily decreased at most altitudes (Fig. 15a) and this was coincident with L1 moving out of the analysis box. R1 re-intensified its updraft by 50 min (Fig. 15a). At the same time, the boundary moved toward the southwest (towards the domain's left edge). As R1 moved closer toward the boundary, it began showing features characteristic of a supercell. For example, a prominent hook-echo began to form by 113 min as the storm crossed the boundary (Fig. 14). R1's updraft grew in volume as it approached and crossed the boundary (Fig. 15c-d). Almost immediately upon crossing, other convection began forming NW of R1. The convection formed on R1's NW side but this convection was mostly transient and no convection formed within R1's inflow region. Simulated reflectivity continued to

increase with height from 70 to 100 min where it remained steady for the remainder of the simulation (Fig 15b). As the storm crossed into the new environment, the updraft deepened as the top of the 5, 25, and 40 m s^{-1} updraft contours increased with height. The updraft also increased at low levels, at least briefly during boundary crossing, as indicated by the lowering of the bottom of the 15 m s^{-1} updraft contour. The vertical vorticity also developed closer toward the ground as the storm crossed into the new environment (100 min; Fig. 15e), indicating an increase in low-level rotation. R1 began to deviate toward the right (in a natural coordinate framework) immediately after crossing the boundary and remained moving toward the SE as it increased in updraft volume, precipitation area, and showed a well-defined hook-echo at the end of the simulation (Fig. 14, 15c,d).

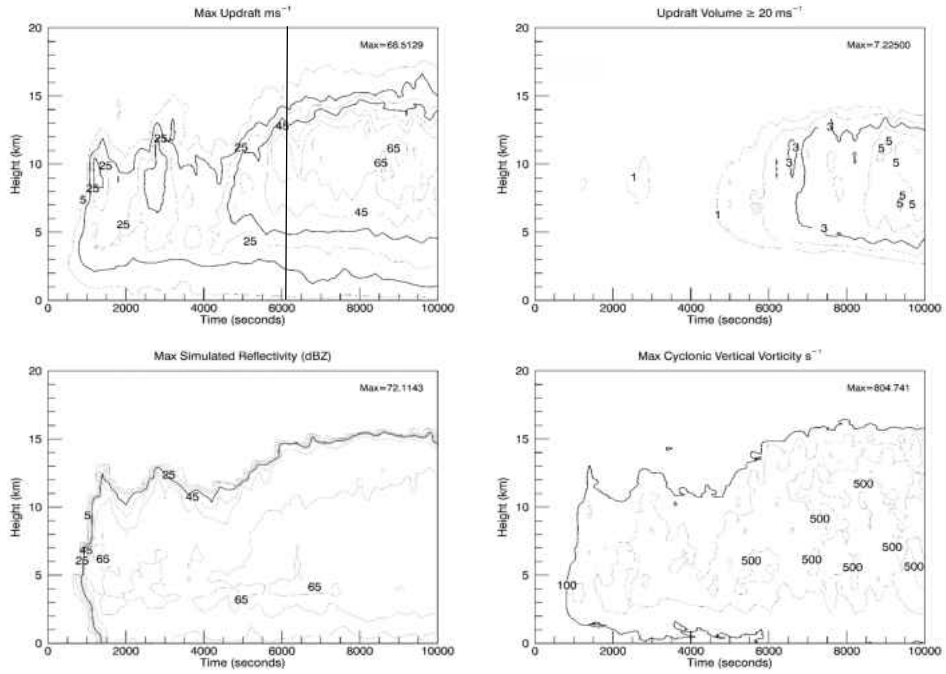

Figure 15. Time-height contour plots of (a) maximum vertical updraft speed (m s^{-1}), (b) maximum simulated radar reflectivity (dBZ), (c) updraft volume greater than 10 ms^{-1} (km^3), (d) updraft volume greater than 20 m s^{-1} (km^3), and (e) maximum cyclonic vertical vorticity (1x10^{-4} s^{-1}) within a box following R1. The black vertical line denotes the time when the storm updraft crossed the boundary (where the boundary is defined by the –1 K potential temperature perturbation) .

Maximum vertical vorticity at the surface, 1km, and 3km is shown in Fig. 16c. The 1 and 3 km vertical vorticity trends were cyclic and no steady pattern is shown. However, the surface vorticity was steady until about 100 min when it increased to .03 s^{-1} where it remained until after the storm crossed the boundary. After boundary crossing, the surface vorticity remained higher than pre-crossing values. Thus, indicating that the storm was in a more favorable environment for low-level rotation. The 2-5 km updraft helicity increased rapidly from 100 min up until the time the storm completely crossed the boundary (Fig 16b). The helicity decreased dramatically after boundary crossing but remained higher than pre-crossing values.

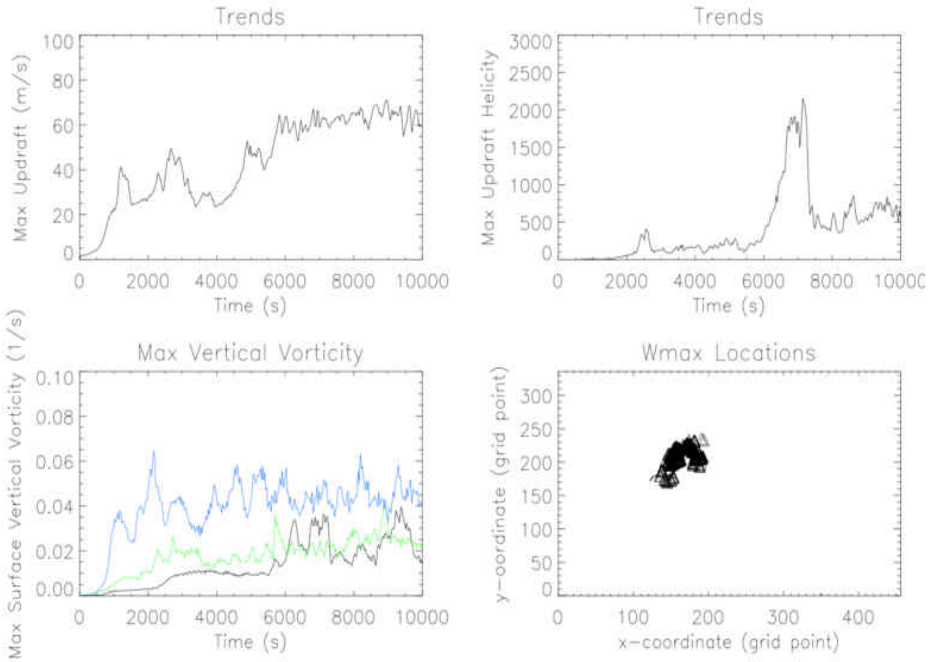

Figure 16. Trend plots for R1 of the control simulation for (a) maximum updraft (m s^{-1}), (b) 2-5 km updraft helicity (UH) (m^2 s^{-2}), (c) maximum vertical vorticity (s-1) at z = 3 km (blue), z = 1 km (green), and z = surface (black), and (d) maximum domain-relative updraft locations within model.

Kinematic Analysis

It is useful to take a closer look at some of the properties of R1 (referred to as "storm," hereafter) as it evolved with time and crossed into the new environment. One question the reader might ask is why vorticity values decreased again after the storm crossed the boundary since the storm should have been in a more favorable environment for low-level rotation. This will be further explored by looking at the vorticity, vertical motion, and horizontal wind fields at several different vertical levels as the storm went from one environment to the other.

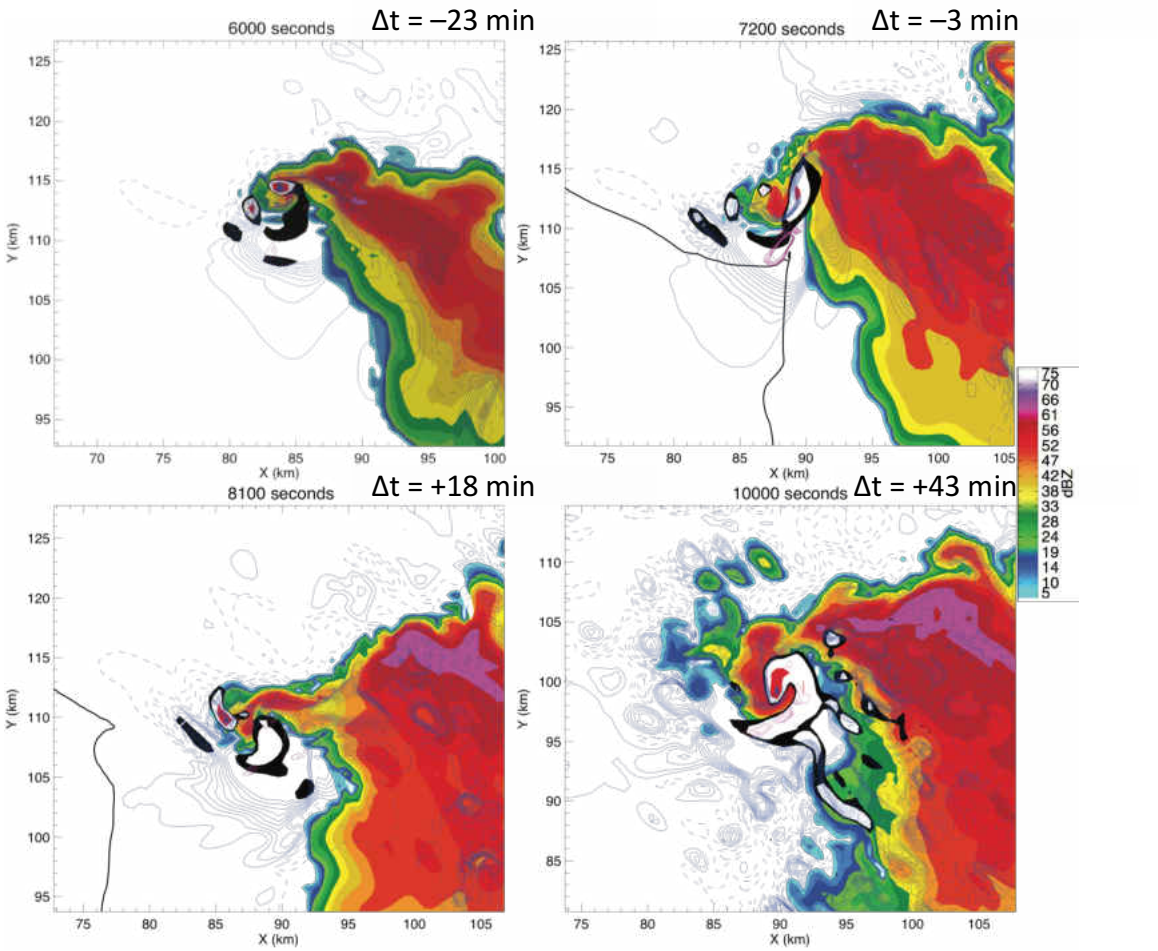

Figure 17. Simulated radar reflectivity at z = 3 km. The black contours denote the –1 K surface theta perturbation from the base state sounding. Blue contours are updraft values at z = 3 km (solid for positive values and dashed for negative values) for 1 m s^{-1} to 10 m s^{-1} at 1 m s^{-1} intervals. Shaded contours are vertical vorticity at z = 3 km (only positive values contoured) starting with 0.005 s^{-1} (black) and then 0.01-0.1 s^{-1} with an interval of 0.01 s^{-1} (note that white inside the black contour is 0.01 s^{-1} and does not mean no value). The magenta contours denote updraft helicity.

Figure 17 shows horizontal cross sections at 3 km as the storm moved toward and past the boundary. The updraft was well established at $\Delta t = -23$ min as the greatest vertical velocities remained immediately on the NW side of the rear flank gust front, where a large gradient of vertical velocities was located. Strong vertical velocity gradients are known to play an important role in horizontal vorticity being tiled vertically. At $\Delta t = 0$, vorticity at 3 km expanded in area and 2-5 km helicity increased (not shown) along the juxtaposition of the updraft, rear flank boundary, and preexisting boundary. This is still seen at $\Delta t = -3$ min. The updraft was nearly centered where the preexisting and rear flank boundaries intersected each other. Notice the RFD and hook appendage were wrapping into the updraft by $\Delta t = 43$ min. Also, it is noted that vertical vorticity increased within the same area. This region was experiencing large vertical velocity gradients and a strong updraft, aiding in production of cyclonic vertical vorticity by tiling and stretching of horizontal vorticity (not shown).

While the 3 km level updraft was well established, it was mentioned previously that low-level vorticity values decreased again once the storm crossed the boundary. Figure 18 shows trends closer to the ground ($z = 500$ m). Similar to Fig. 17, the 500 m updraft was on the NW side of the rear flank gust front. Notice the kink in the rear-flank boundary, as this was an area were surface convergence was occurring (not shown). A vertical vorticity maxima was collocated with the updraft along this kink. As the storm crossed the boundary, the kink was then centered at the intersection of the rear flank and preexisting boundaries. At the same time, the updraft broadened and was concentrated in the same location. The vorticity maximum appeared to be cut off at $\Delta t = +2$ min and a new vorticity maximum and updraft began to form farther NE at $\Delta t = 5$ min. By the end of the simulation,

the low-level updraft and associated vorticity had similar patterns to the 3 km level (not shown).

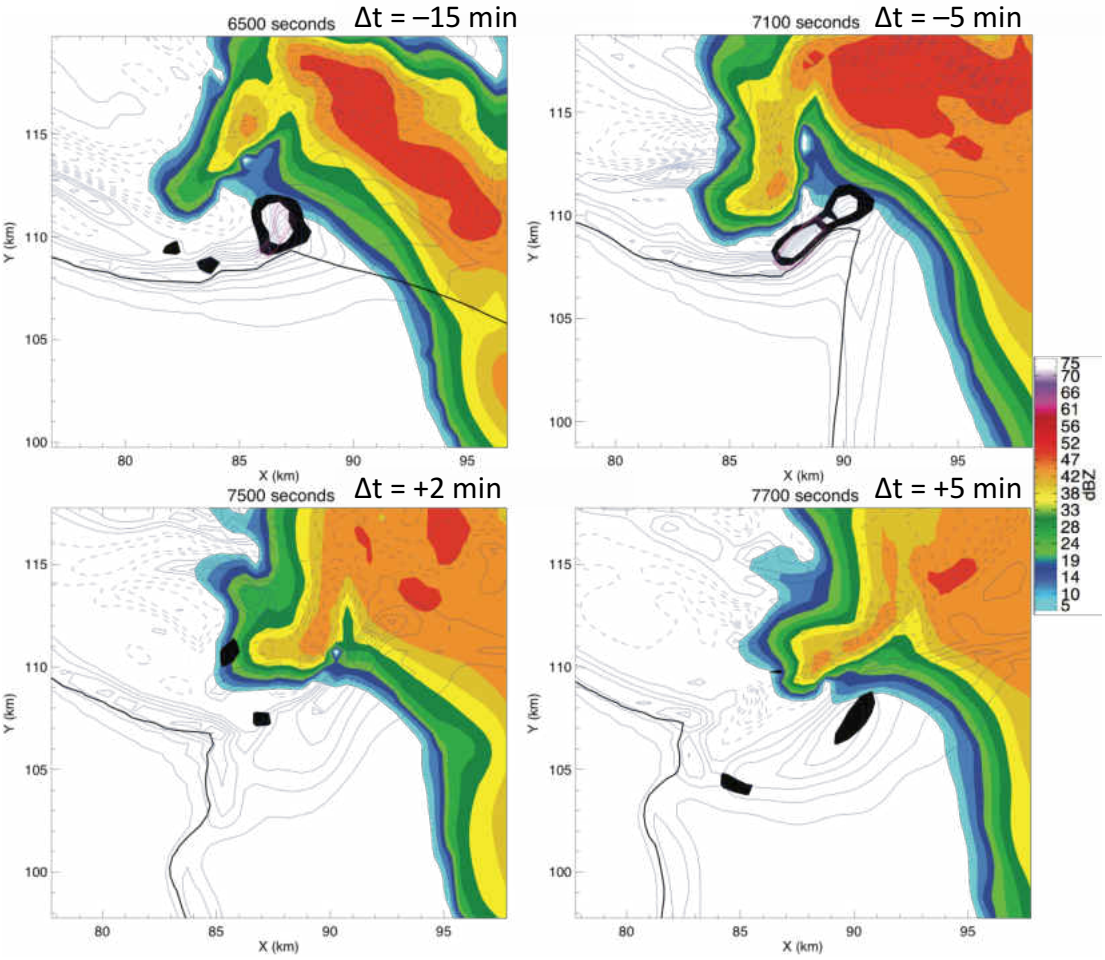

Figure 18. Same as Fig. 17 but for z = 500 m.

Figure 19 shows a closer look at the apparent reorganization of the low-level mesocyclone region as the boundary and storm moved past each other. At Δt = –11 min, the kink in the rear flank boundary continued to deepen as the preexisting boundary approached. The vorticity and updraft followed along the kink and appeared to be quite broad as the boundary moved close (Δt = –5 min). In the short time span from Δt = –5 min to Δt = 0 min, the low-level mesocyclone shrank in size immediately at Δt=0 and was gone

be Δt = 3 min (not shown); thus, the redevelopment of the low-level updraft is shown at Δt = 7 min, where it continued to increase closer toward the hook echo at later times.

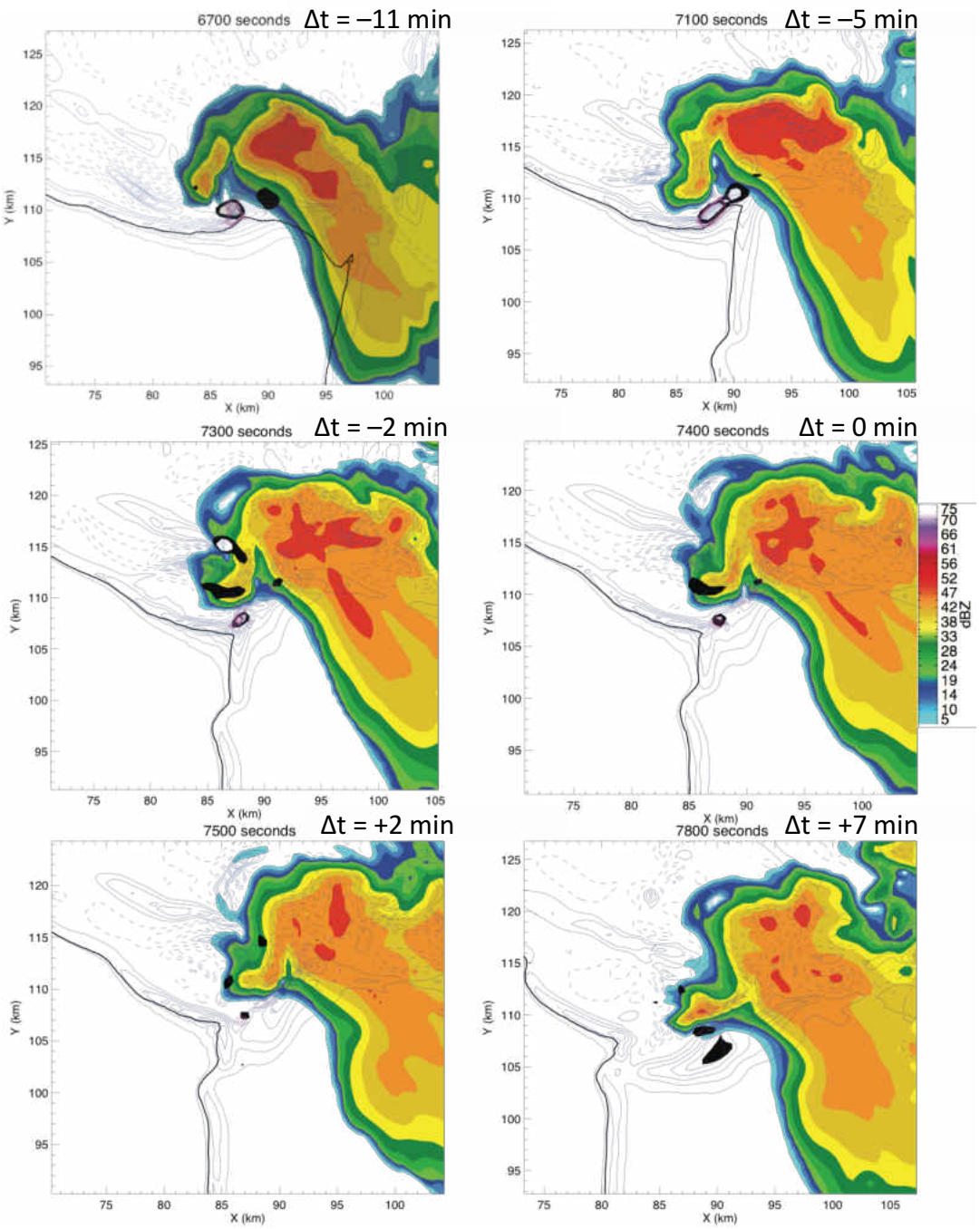

Figure 19. Same as Figure 18.

Sensitivities

While the results of the above section show some insight into the processes that took place when the storm crossed the boundary, it is useful to validate the robustness of the results. Does the storm always increase in intensity as it crosses, or was it a coincidence? A sensitivity analysis also helps to show if the results would be similar at different times in a storms lifecycle. Recall that Figure 12 shows the warm bubble and boundary placement at time=0 for all simulations discussed in this section. Each simulation has the naming convention Δx_time_B, where Δx is the distance between the warm bubble and boundary (denoted by the -1 K theta perturbation contour) at time = 0, time represents the model time at boundary crossing, and B indicates the percentage of the way across the domain the boundary was initialized.

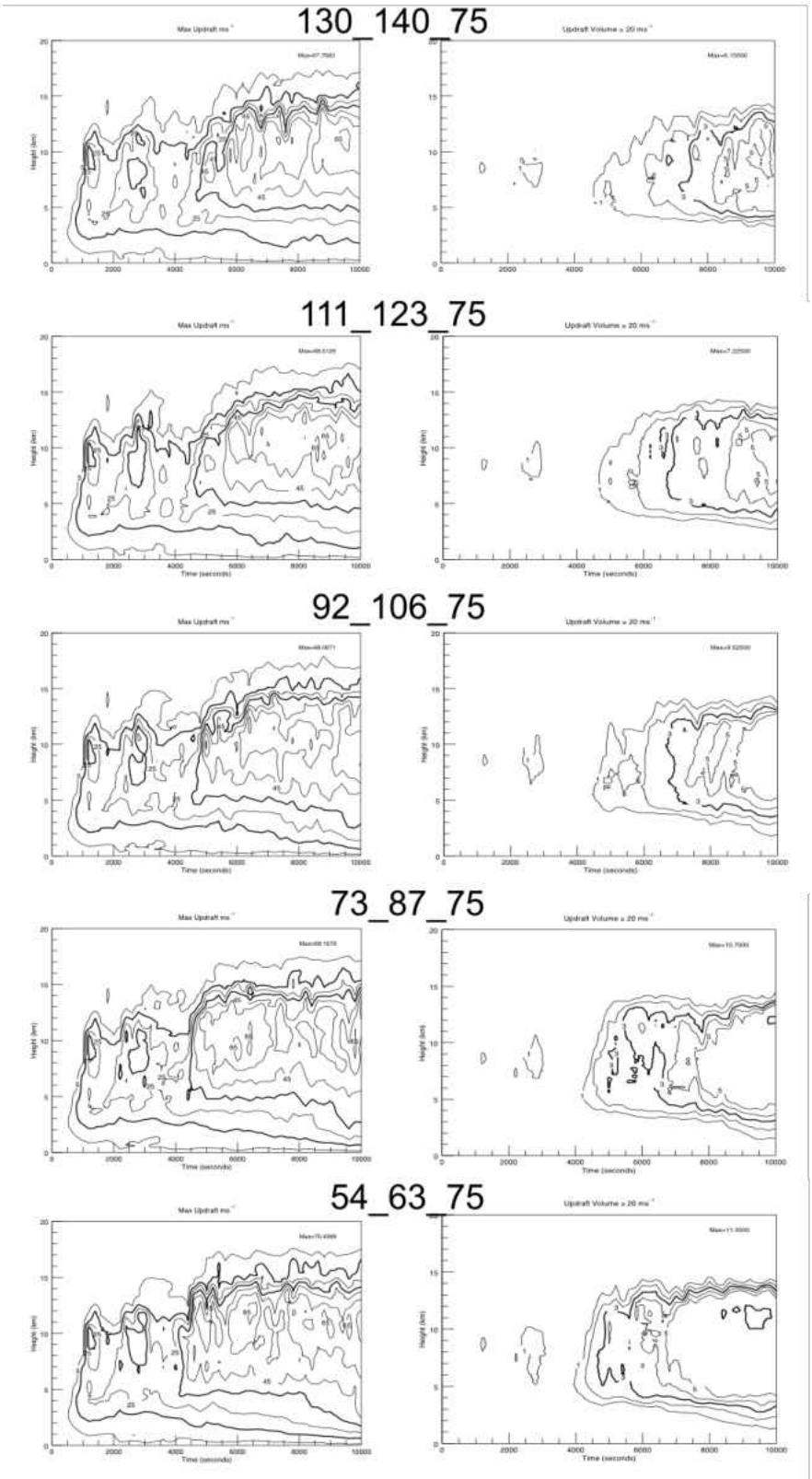

Figure 20. Same as Fig. 15 except only showing maximum updraft and updraft volume greater than 10 m s^{-1} for the five different simulations (see Fig. 12).

The five simulations show variations in storm updraft maxima (Fig. 20a). Unsurprisingly, the storms all showed similar behavior in the first 30 minutes of the simulations; however, after each storm split into the right- and left- moving supercells, differences in the updraft evolution occurred. In each of the simulations the right mover updraft increased in height and then decreased again before each model solution diverged (time of storm splitting). At around 70 minutes the storm updraft increased again but the structure of each solution is different in the time height plots. In the 130_140_75 and 111_123_75 cases, the crossing happened well after the updraft increased to a steady state. There are no clear indications that the updraft structure was affected by the cross into the new environment within the upper levels; however, the bottom 15 ms^{-1} updraft contour did lower in each of these cases before $\Delta t=0$, indicating a brief increase in the low-level updraft. This seems to align with the previous result that that low-level updraft was increasing (along with vertical vorticity) along the rear flank boundary kink leading to $\Delta t = 0$ min (Fig. 18). In the other three simulations, all with smaller Δx values, the updraft increase with height was much more abrupt than in 130_140_75 and 111_123_75 simulations (Fig. 20a). The storms from 73_87_75 and 54_63_75 were already at and behind the boundary at the time of the abrupt updraft increases, respectively.

The updraft volume of ≥ 20 ms^{-1} showed stark differences between each of the simulations (Fig. 20b). In all the simulations, the updraft volume ≥ 20 ms^{-1} increased during or after the boundary crossing. In the storms that moved into the new environment early in the simulations, the updraft volume increased earlier than in the simulations where the storm remained in the warm side environment longer.

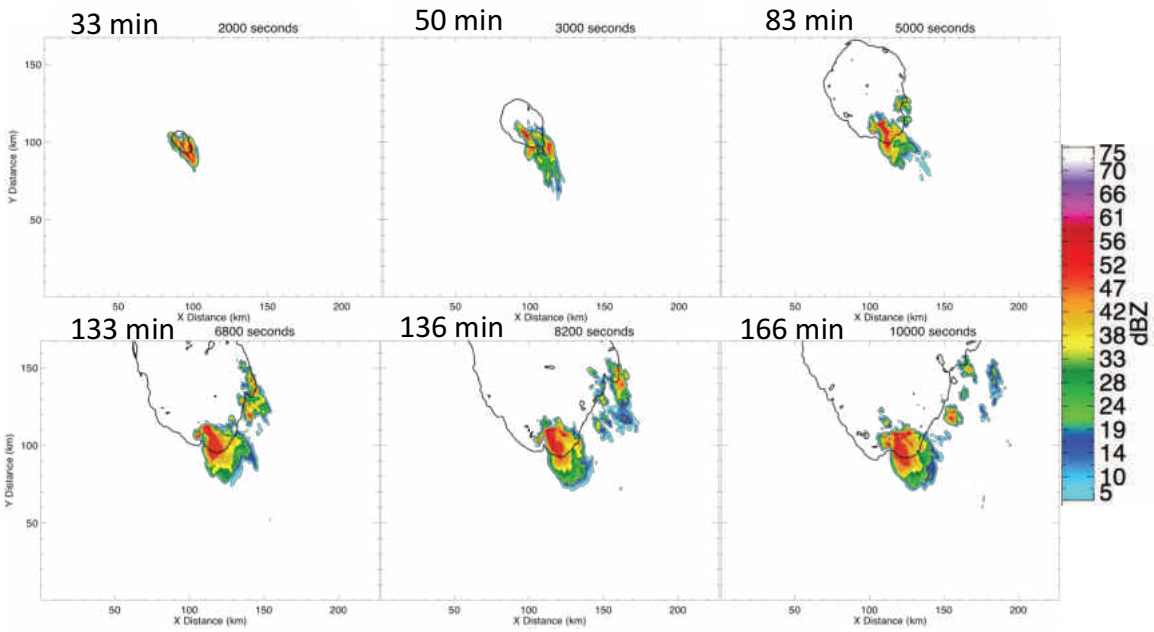

Figure. 21 Simulated reflectivity horizontal cross sections at z = 1.5 km. The black contours denote the -1 K surface theta perturbation from the base state sounding.

A homogeneous warm side simulation was performed to see how it behaved in comparison with the boundary crossing storms. Figure 21 shows the same simulated reflectivity cross sections as shown for the control case (Fig. 14). The warm side run exhibited similar trends in its morphology in the early stages of the simulation. However, unlike the boundary crossing storms, it did not turn as much toward the right at any given point in the simulation. In addition, the updraft volume ≥ 20 ms^{-1} was much different than any of the boundary simulations (Fig. 20,22), showing that the storms that crossed the boundary had larger updraft volumes. The WarmRun storm continued to increase in updraft volume and showed a hook echo up until t=10000 s. By time=12000 s, the WarmRun storm became cold pool dominant and more linear without a hook echo (not shown).

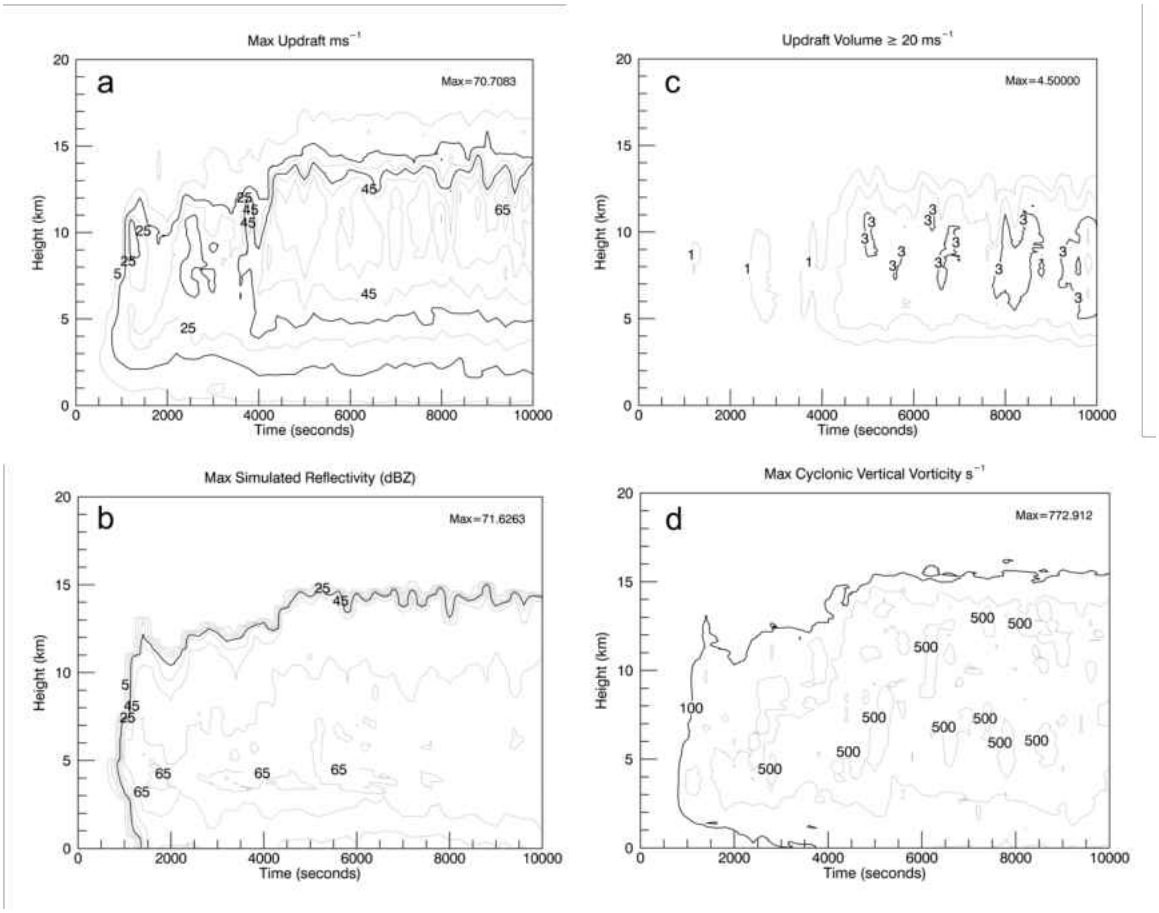

Figure 22. Time-height contour plots of (a) maximum vertical updraft speed (ms^{-1}), (b) maximum simulated radar reflectivity (dBZ), (c) updraft volume greater than 10 ms^{-1} (km^3), (d) updraft volume greater than 20 ms^{-1} (km3), and (e) maximum cyclonic vertical vorticity ($x10^{-4}$ s^{-1}) within a box following R1

Figure 23 shows simulations 130_140_75, 111_123_75, and 73_87_75. No matter the storm age, between times Δt=-7 and Δt=5 min, new updrafts developed at low-levels, as the preexisting boundary and rear flank gust front collided and caused the established low-level updraft and mesocyclone to dissipate. In 73_87_75, the low-level updraft was not as pronounced as the other two simulations shown. This storm was only approximately 80 min old, whereas the other two were 133 and 117 minutes old, respectively. In the cases here (and other cases discussed above in Fig. 20a,b), even if the low-level updraft and

mesocyclone were well established, a new updraft began to from immediately after the boundary crossed the storm and cut-off the established low-level updraft/mesocyclone.

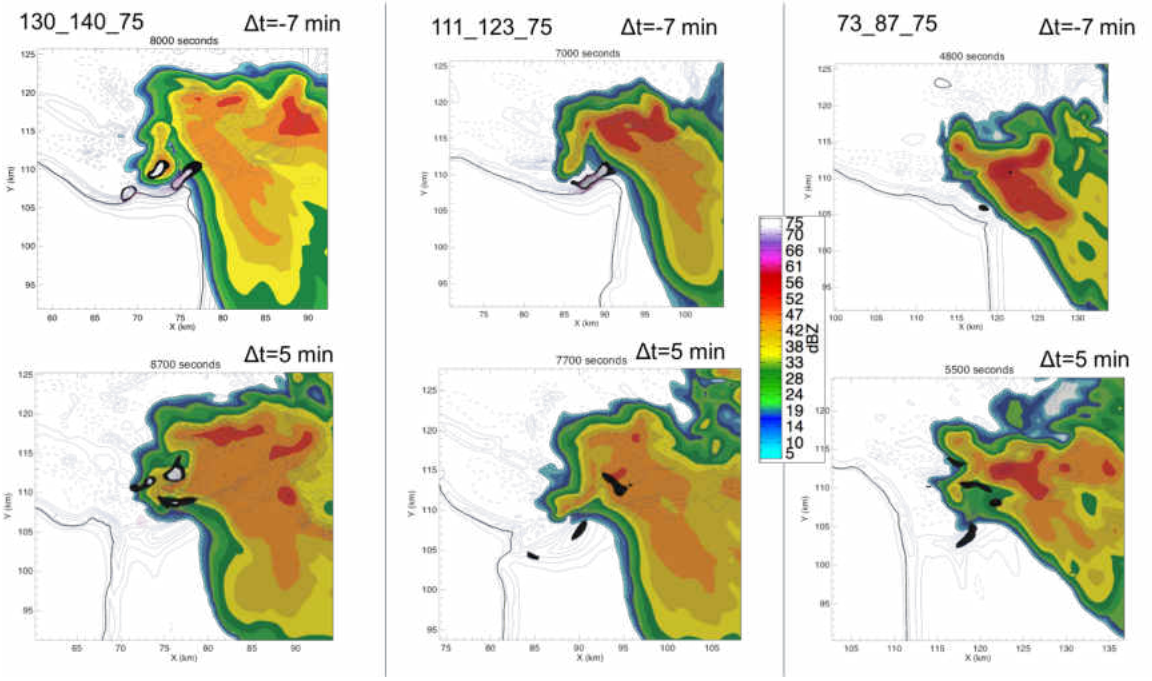

Figure 23. Simulated radar reflectivity at z = 500 m. The black contours denote the -1 K surface theta perturbation from the base state sounding. Blue contours are updraft values at z = 500 m (solid for positive values and dashed for negative values) for 1 m s $^{-1}$ to 10 m s $^{-1}$ at 1 m s $^{-1}$ intervals. Shaded contours are vertical vorticity at z = 500 m (only positive values contoured) starting with 0.005 s $^{-1}$ (black) and then 0.01-0.1 s $^{-1}$ with an interval of 0.01 s $^{-1}$.

The 2-5 km updraft helicity was a good indicator of how this restructuring process affected the storms. In Fig. 24, runs 130_140_75 and 111_123_75 increased in helicity from around 400 to over 2000 m^2s^{-2} at t=100 min. In both cases, this occurred before the storm crossed the boundary. In the WarmRun simulation, a similar increase happened around the same time. In run 92_106_75, there was also a similar increase in UH, but the increase was not as significant as in 130_140_75, 111-123_75, and WarmRun simulations. In 111_123_75 and 93_106_75, the UH decreased immediately after crossing the boundary, while 130_140_75 was in a local minimum as the storm crossed the boundary. Runs 73_87_75 and 54_63_75 showed differences in UH compared to the other simulations. There was no increase around t=100 min as the storm had already crossed the

boundary and was in the cool side environment by that time. However, both 73_87_75 and 54_63_75 began to increase significantly in UH at Δt=64 min as both storms had been in the cool side environment more supportive of low-level rotation and updraft velocity (higher CAPE and backed surface winds). Similar patterns in vertical vorticity are shown in Fig. 25 for all cases. In 54_63_75, the storm that crossed the boundary at the youngest age, vertical vorticity values began to increase to values greater than all runs, including WarmRun.

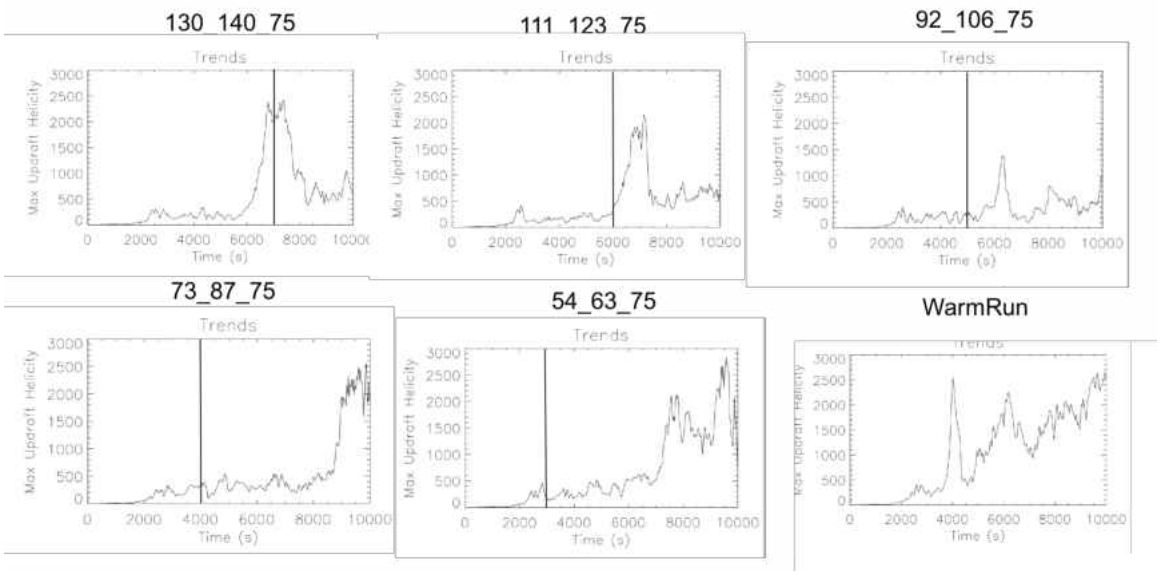

Figure 24. Trend plots of 2-5 km updraft helicity (UH) ($m^s\ s^{-2}$) for each of the five boundary simulations and the homogenous warm side simulation. The vertical black line denotes when the storm crossed the boundary.

One other sensitivity test was performed to test the validity of the cold pool location at t=0. Since the boundary placement within the model domain effectively changes the mass, a run was performed where the boundary was implemented at 85 percent of the way across the domain's x-axis. In other words, the low-level cold pool was only in 15 percent of the model domain at t=0. Figure 26 shows the 130_140_75 simulations compared with the 130_140_85 run. For this, the Δx value (130 km) was kept constant, such that the storm

and boundary should still cross each other at the same time. Indeed, the storm crosses the boundary at the same time in both cases. The updrafts show similar patters with height.

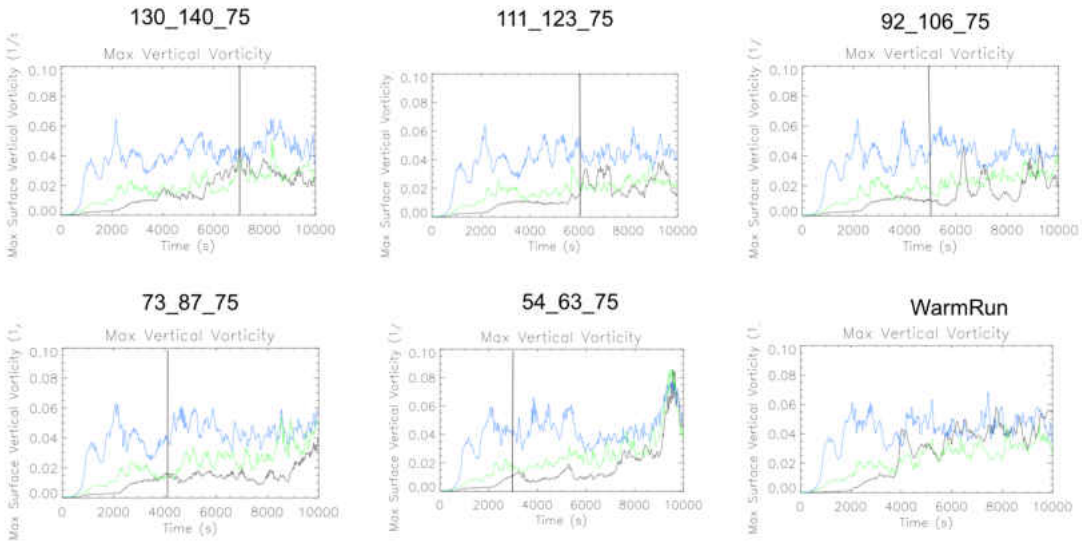

Figure 25. Trend plots of maximum vertical vorticity (s^{-1}) at z = 3 km (blue), z = 1 km (green), and z = surface (black) for each of the five boundary simulations and the homogenous warm side simulation. The vertical black line denotes when the storm crossed the boundary.

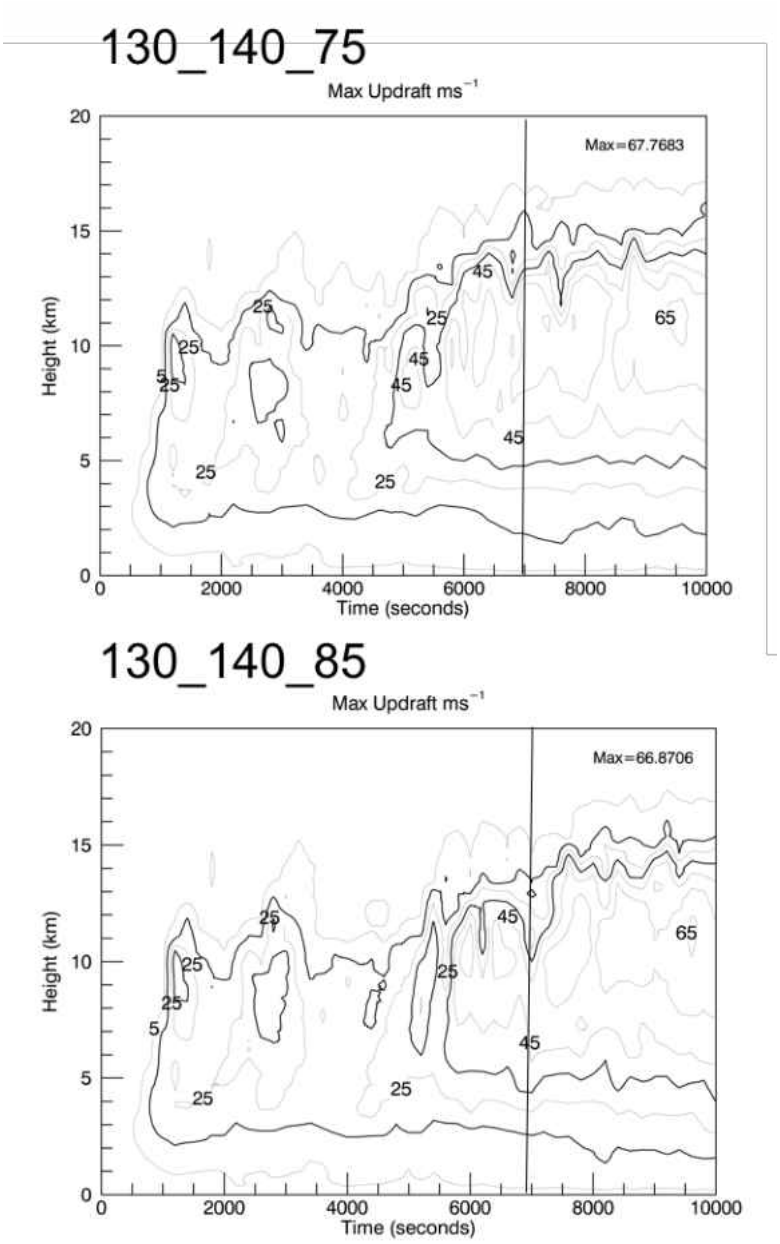

Figure 26. Time-height contour plots of maximum vertical updraft speed (m s^{-1}) for Δx = 130 for both simulations where the boundary was initialized at 75 % and 85 % of the way across the model's x-domain. The black vertical line denotes the time when R1 crossed the boundary.

Readjustment and Sensitivity Discussion

The low-level mesocyclone readjustment process happened in all cases, no matter the storm age. A few comments are in order regarding this result. Before the boundary crossing, the low-level updraft was established along the rear flank gust front. This may have been feeding low-level air into the mid-level updraft, potentially acting to tilt horizontal vorticity and providing warm moist air into the mid-levels of the storm. As the preexisting boundary collided with the rear-flank boundary, the mass of the preexisting boundary may have swept away the low-level updraft/mesocyclone. Keep in mind that the preexisting boundary was only below 2.4 km, so the 3 km updraft would not be swept away. Even the 1 km and 2 km level updrafts did not experience the same cut off, likely due to the upper levels of the boundary not being as pronounced as it was closer toward the surface.

It is not clear that the low-level updraft/mesocyclone readjustment result is robust for all situations in nature where a storm crosses a preexisting boundary. It is hypothesized that certain factors such as, speed, angle of storm and boundary, height of the cold pool, and baroclinic differences may be contributing factors to the processes of the low-level readjustment. For example, if a storm moved as a so called "boundary crawler" and travelled along a boundary, it may be possible that the low-level updraft/mesocyclone would remain intact since the boundary would not be pushing past the storm. Atkins et al. (1999) discussed boundary crossing storms with regard to crossing angle and found that storms which crossed more perpendicular to the boundary had lower values of low-level vertical vorticity. While they referred to the lack of time the storm updraft had to gain streamwise horizontal vorticity from the baroclinic zone of the boundary, this study

suggests the restructuring of the low-level updraft/mesocyclone to be another impact on the storm vorticity.

In all cases, the storm turned toward the right upon crossing the boundary. All cases showed that the storm movement continued toward the SE well after crossing time. This change in movement from one environment to the other is explained by the change in the 0-6 km mean wind. At the lowest levels, the winds backed on the cool side of the boundary, thus the average storm motion turned more toward the right. This storm motion change should have also had an impact on the streamwise horizontal vorticity available for the updraft to ingest.

The period between boundary crossing and intensification of low-level rotation is of interest not only to researchers, but also to operational meteorologists. The main question revolves around whether there is a certain length of time after crossing before storms increase in rotation again? Could it also depend upon storm age?" Looking back at Fig. 24, after the storms crossed and began their intensification at low-levels, there was a fairly uniform amount of time for 73_87_75, 54_63_75, and 130_140_75 to increase in UH (about 60 min). The 130_140_75 simulation showed an increase in UH by 30 min after crossing. While not clear cut, the oldest storm did regain higher UH values quicker.

In the time-height plots (Fig. 22), there was not always obvious signs that the storm had crossed into the more favorable environment. However, even though all storms increased at around t=67 min, the increase in the upper levels did not show the same pattern for each storm. For example, in 130_140_75 the upper 15 ms^{-1} updraft contour slowly increased from about 75 to 115 min. The 73_87_75 simulation upper 15 ms^{-1} updraft contour increased much quicker from 75 to 80 min. Perhaps the quick increase in updraft

with height in 73_87_75 and 54_63_75 simulations at t=75 min was due to the more favorable low-level environment on the cool side of the boundary; thus, another important characteristic to keep in mind for operational meteorologists.

Vorticity Analysis

While it has been shown that the boundary does impact the low-level mesocyclone of the storm, there is still a lack of understanding of the air coming into the storm from both a qualitative and quantitative view. The trajectory analysis provides a mechanism to fit these pieces of the puzzle. The goal of trajectory analysis is to determine if vorticity is processed differently from the two different environments that are used in the study herein.

Figure 27 shows a plan view at z = 500 m of the 92_106_75 storm at a time (a) before and (b) after the storm crosses the boundary. The times shown are when the trajectories were released within the mesocyclones. Note that the after crossing 500 m mesocyclone possess greater values of vertical vorticity compared to the before crossing case (Fig. 27 a,b). In the after crossing case, the storm is generally larger and displayed a well-established hook appendage. The wind displayed within the analysis box shows both mesocyclones had convergence toward their centers, with more cyclonic motion shown in the after crossing mesocyclone (Fig. 27a,b).

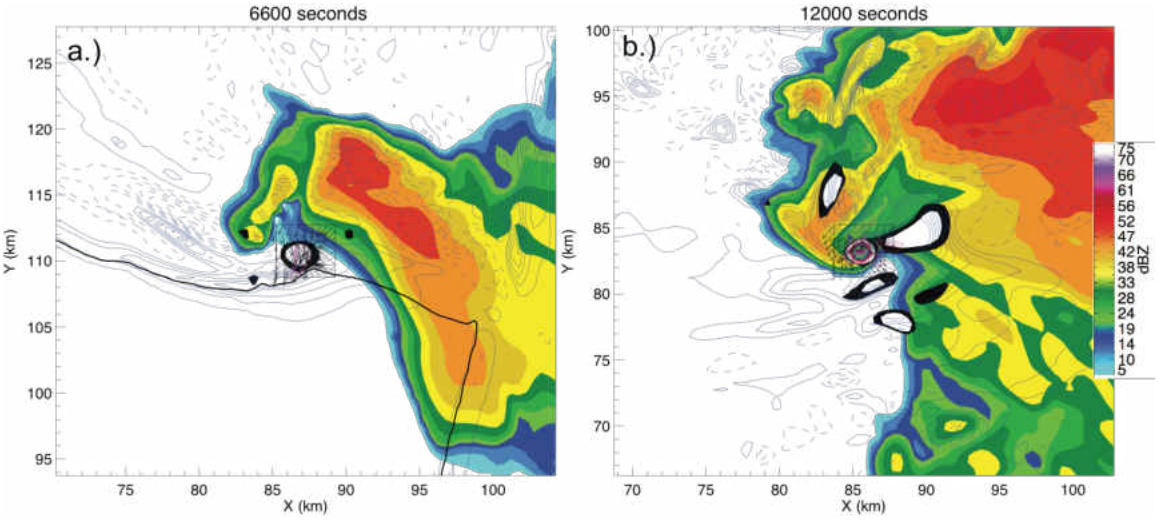

Figure 27. Plan view at z=500m for before crossing (a) and after crossing (b) case.

The trajectory paths are shown three dimensionally in Fig. 28. The before crossing case had 21 rising and 79 descending trajectories, while the after crossing case had 42 rising and 58 descending trajectories. Clearly, the descending trajectories contributed more to the mesocyclone in the before crossing case, but also, trajectories came from higher aloft on average as compared to the after crossing case. These differences in trajectory makeup and source region are important and warrant further analysis.

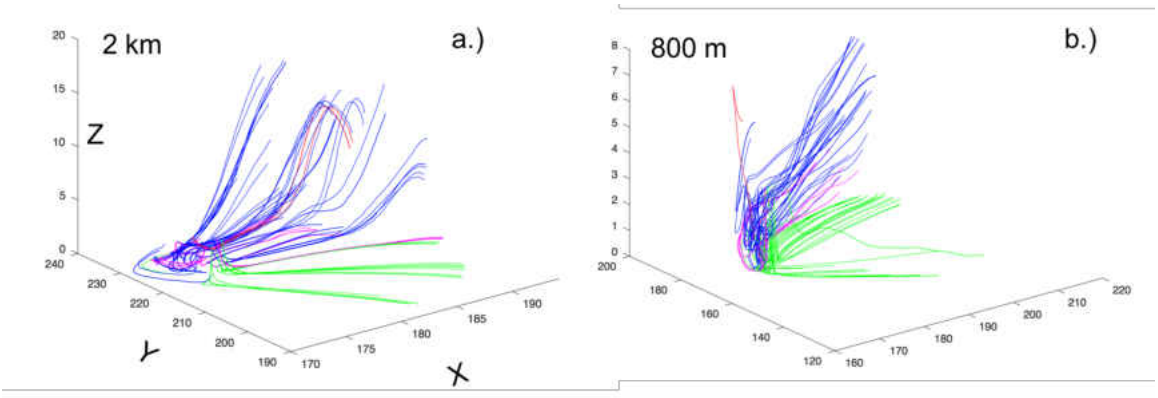

Figure 28. 3D view of before (a) and after (b) crossing case. Blue are the descending trajectories and green are rising trajectories.

Figure 29 shows the quantitative results of the calculations of vorticity components along the trajectory paths for the average rising trajectory from each case, where time = 0 represents when the trajectory is 900 s from its final position. Both cases show similar paths with height, as both trajectories stayed below 50 m until about 800 s when the after crossing case rose above 50 m and ascended into the mesocyclone. The before crossing case shows the same pattern but resided below 50 m for a slightly longer period (Fig. 29a). The vertical vorticity stayed near zero for both cases until the trajectories began slight rising trends with height (Fig. 29a,b). This is shown in the stretching of vertical vorticity that is proceeded by positive tilting of horizontal vorticity into the vertical (Fig. 29c,d). Remember vertical vorticity stretching cannot occur until vertical vorticity is present; thus, it is shown that as the trajectories began to start their ascent, tilting of horizontal vorticity gave rise to vertical vorticity that was then amplified via stretching in conjunction with the increase in vertical velocity (Fig. 29c,d,e).

The absolute horizontal vorticity was initially higher in the after crossing case, as that environment possessed more horizontal vorticity simply from the input sounding (Fig. 29f). With more initial horizontal vorticity, the after crossing trajectory had more stretching of horizontal vorticity as compared to the before crossing trajectory (Fig. 29g). Baroclinic generation tendencies were comparatively similar for both trajectories, having gradual upward trends until 600 s when the before crossing trajectory began to increase rapidly in baroclinic generation. The after crossing trajectory also shows an increase but the overall magnitude of the increase was less than the before crossing case (Fig. 29h).

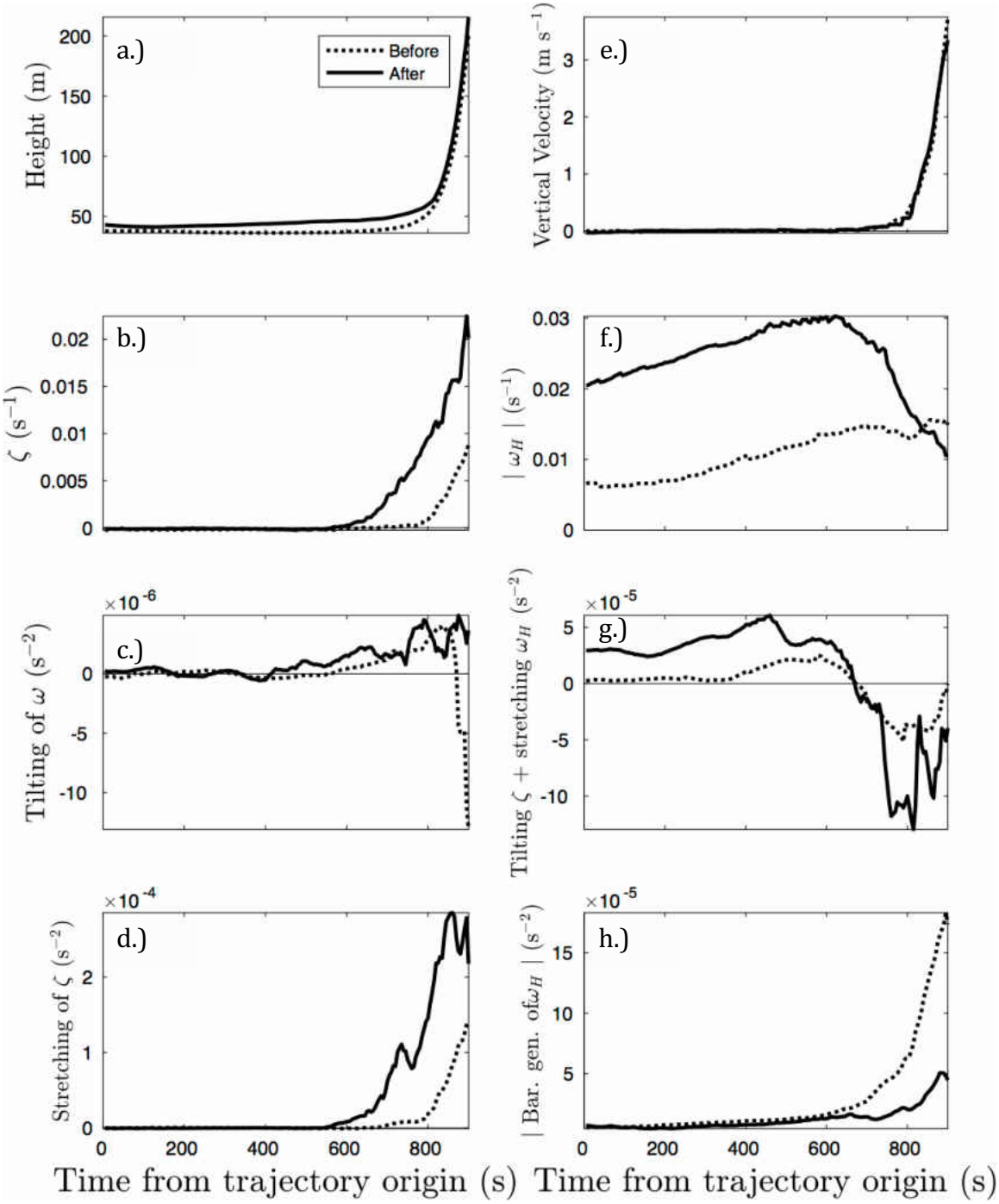

Figure 29. Composite trajectories for the before (dashed line) and after (solid line) cases of (a) height, (b) vertical vorticity, (c) tilting of horizontal vorticity into the vertical, (d) stretching of vertical vorticity, (e) vertical velocity, (f) magnitude of the horizontal vorticity vector, (g) tilting of vertical vorticity into horizontal vorticity plus stretching of horizontal vorticity, and (h) magnitude of baroclinic generation of horizontal vorticity. The x axis indicates the 900 s time the trajectory was tracked backwards in time with 900 s indicating the final position of the trajectory in the mesocyclone.

The descending trajectories were calculated in a similar way as the rising trajectories, with the exception that we are now only looking at the 400 s window centered around when the average trajectory for each case reaches below 100 m. As was shown in Fig. 28, the average trajectory for the before crossing case descended from higher aloft as compared to the after crossing case (Fig. 30a). Both cases had negative vertical vorticity during descent to 100 m; however, there is a clear difference in the trend of vertical vorticity as the trajectories approached 100 m (Fig. 30b). In the before crossing case, vertical vorticity became less negative and turned positive 50 s before reaching 100 m. As the trajectory approaches 100 m, its velocity slowed (Fig. 30e) and stretching of vertical vorticity became less positive; thus, vertical vorticity began to become less negative and eventually positive in the last 50 s before reaching 100 m (Fig. 30b,c,d). This agrees with the notion that a decrease in stretching (as the trajectory descends toward the surface it slows down) of negative vorticity will make it less negative. In the after crossing case, vertical vorticity remained negative well after reaching 100 m. For this case, the tilting of horizontal vorticity into the vertical had steadily increased and then vertical stretching increased rapidly as it entered the mesocyclone (Fig. 30c,d). The after crossing case acquired horizontal vorticity via continuous stretching throughout most of its path toward the mesocyclone and possessed more horizontal vorticity 75 s after reaching 100m as compared to the before crossing case (Fig. 30f,g). This steady increase in horizontal vorticity then contributed to the final value of vertical vorticity by tilting and stretching into the vertical in the last 75 s.

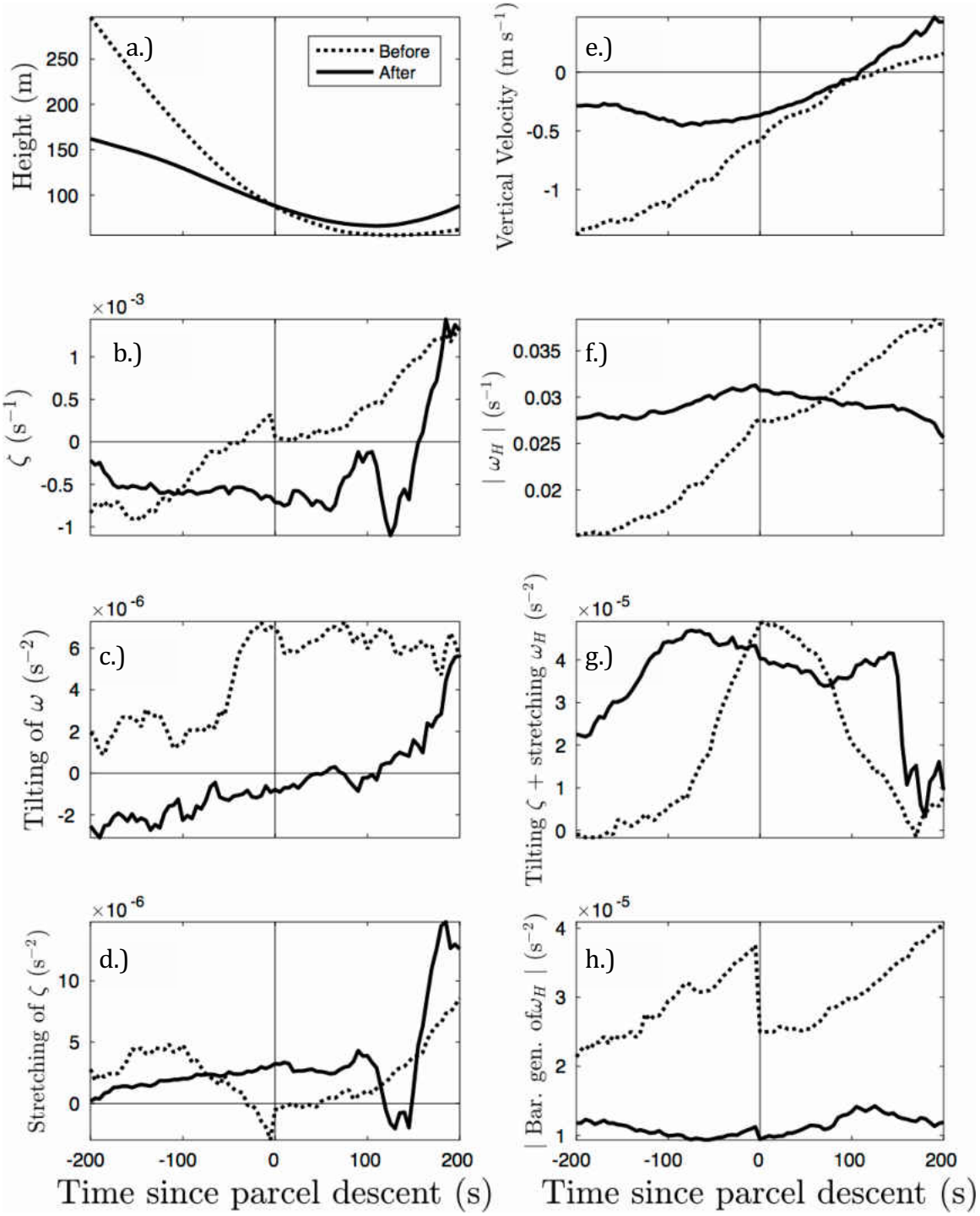

Figure 30. Same as Fig. 29 except for descending trajectories. Only 400 s of the 900 s path is shown and is centered around trajectories first reaching the 100 m vertical level.

Vorticity Summary & Discussion

The case presented here shows that the rising trajectories were similar in the way vorticity was processed for both the before and after crossing trajectories. The after crossing case rising trajectory had a higher ending vertical vorticity value likely owing to more initial horizontal vorticity (from the initial environment) and then more tilting of vorticity from the horizontal to the vertical that was then stretched more as it entered the mesocyclone, as compared to the before crossing case. Thus, the rising trajectories yield a result that one would expect simply based on the two different sounding profiles used to initialize each side of the boundary (i.e., more low-level vertical shear and more CAPE on the cool side).

The descending trajectories elucidate differences between the before and after crossing cases. The paths of approach from both the trajectories were different and likely played an important role in vorticity production. In the before crossing case, it was shown that there was a decrease in stretching of vertical vorticity as the trajectory approached 100 m; thus, the negative vertical vorticity acquired during the descent began to become less negative. As the trajectory travels more parallel to the surface, horizontal stretching increased. This was then tilted and stretched vertically as the trajectory began to rise towards the mesocyclone. In other words, the vertical vorticity acquired during descent was re-oriented into the horizontal, stretched, and then tilted into the vertical again before entering the mesocyclone. The after crossing case was quite different, in that it acquired most of its horizontal vorticity via stretching in the horizontal and was subsequently tilted and stretched vertically as it approached the mesocyclone.

The differences in the before and after crossing descending trajectories show that the differing environments do alter the way vorticity is produced. While tilting and stretching into the vertical are clearly important in the final seconds before the trajectories enter the mesocyclones, the amount of horizontal vorticity available to be tilted and subsequently stretched may depend on the way the trajectory descends. These findings are summarized below:

1) For descending parcels that come from higher aloft (descend at a steeper rate), titling of horizontal vorticity into the vertical is oriented such that it is negative vertical vorticity, but reorientation to positive vorticity occurs after descending below 100 m
2) For descending parcels that are shallower and travel with a smaller angle toward the surface, the available horizontal vorticity from the environment is stretched horizontally before being tilted and stretched vertically
3) The amount of contribution from both the rising and descending trajectories may be of importance, as well. In the before crossing case, about 80 percent of the trajectories seeded in the mesocyclone were from the descending category. In contrast, the after crossing case had about 60 percent descending trajectories. The descending trajectories are made up of downdraft air from the rear-flank of the storm, and as the storm crossed into the cool side environment, the CIN increased and was likely the major factor in decrease in not only the number of descending trajectories, but also in the lowering of altitude of trajectory source region. The rising trajectories come from both the storms forward flank and warm inflow region to the southeast of the mesocyclone. In the after crossing case, the rising trajectories

had greater ending values of vertical vorticity as compared to the before crossing trajectories. There were 20 percent more rising trajectories in the after crossing case (as compared to before crossing) and since those trajectories also had greater ending values of vertical vorticity, it can be inferred that the rising trajectories in the after crossing case played a more important role than they may have in the before crossing case. This underscores the sensitivity there may be with regard to CIN and low-level rotation (see Chapter 5 for suggested future work).

CHAPTER 4

CONCLUSIONS

The CM1 model was successfully modified to allow for a horizontally non-homogeneous environment to be initialized. This allowed for the replication of a preexisting outflow boundary within the model domain to move similarly to the observed 2 June 1995 case and modeling study by Fierro et al. (2006).

It was shown that storm and boundary interactions may be of importance to a storm's low-level mesocyclone and vorticity. With the simulations presented herein, the low-level boundary acted to "shut-off" the low-level mesocyclone as the storm and boundary crossed each other. The low-level mesocyclone re-established itself after the boundary crossing. After the re-establishment process, the storm's updraft volume increased and a well-defined hook appendage developed with increasing levels of vertical vorticity located within the low-level mesocyclone.

A sensitivity study was performed to confirm that the same storm behavior happened even when the storm and boundary crossed each other at different times in a storm's lifecycle. In all simulations, the low-level mesocyclone was "shut-off" and storms strengthened again after crossing, with the storms that crossed sooner having higher values of low-level vorticity toward the end of the model simulations. Likely due to the more favorable supercell environment on the cool side of the boundary. In the single simulation where only the warm side sounding was used to initialize the model (i.e., a standard

research practice), the storm behaved similarly for over half the simulation but gusted out toward the end of the model simulation. This is in stark contrast to all other simulations that crossed the boundary. All storms that crossed the boundary were still showing supercell characteristics at the end of model simulations. Thus, even though all storms in all simulations formed within the same environment, the change in the low-level environment in the simulations had impacts on storm behavior.

The use of Lagrangian trajectory analysis showed that vertical vorticity within the low-level mesocyclone was processed differently before and after the storm crossed the boundary (i.e., moved from one environment to another). With two predominate categories (rising and descending) of trajectories feeding into the low-level mesocyclone, the rising trajectories had similar quantitative trends in vorticity, with the main difference being in higher amounts of vorticity in the after crossing case (Fig. 29). The greatest differences came from the descending trajectories for each case. The differences stemmed from the height at which trajectories descended from aloft. When a trajectory descended from higher aloft (in turn, a steeper rate), it acquired tilting of horizontal vorticity into the vertical that was negative; however, as the trajectory approached the surface, the vertical stretching decreased and the vertical vorticity became positive. This vorticity was then re-oriented into the horizontal as the trajectory travelled more parallel with the surface before being tilted again into the vertical. In the case of descending trajectories travelling more parallel to the ground (trajectories coming from a lower altitude), horizontal vorticity was stretched for a longer period before being tilted into vertically and stretched as they entered the mesocyclone.

The result of the low-level updraft/mesocyclone being "cut-off" is of importance to operational meteorology, as this could lead to a period where a storm is not a tornadic threat. However, these results still need to be tested over a broader range of environmental conditions. In any case, it is still useful for the operational community to be aware of such possibilities. There are other factors that may be involved in how a storm's low-level updraft/mesocyclone behave when such a boundary is nearby. In short, crossing angle, storm and boundary speed, and baroclinic factors are all hypothesized to be potential factors in storm behavior.

In conclusion, the results of this thesis at the very least, highlight the importance of heterogeneous environments that storms may often encounter. While it may not always be possible to detected small-scale changes in the surrounding storm environment, or possible to quantify how a storm's low-level vorticity may change if a boundary is near a storm, the operational meteorologist should be cognizant of such situations.

CHAPTER 5

FUTURE WORK

While the results of the research herein provide some interesting insight into boundary crossing storms, there are several suggested research endeavors for further study on this topic. In no particular order, some suggested future works include: increasing the horizontal resolution of the model to see if the results herein are in agreement at finer grid spacing, alter the thermodynamic profiles to decrease the amount of convective inhibition, and alter the angle at which a storm crosses a boundary.

Several studies have concluded that vertical updraft velocity and storm helicity (vorticity) are highly dependent on model resolution. Therefore, it is recommended that further testing be performed with differing resolutions. In addition, the 500 m horizontal resolution used within the study herein was not sufficient to resolve tornado like vortices, so it is recommended to use a resolution on the order of 100 m (many studies in the literature use 100 m to resolve tornado like vortices).

While it was necessary to increase the CIN within the cool side sounding in order to suppress new storms from forming within the inflow region of the study storm, it would be beneficial to systematically change CIN values to study whether it caused any differences in the low-level mesocyclone cut-off or the trajectory source regions. It is hypothesized that the increase in CIN may have a significant impact on the ability for the

low-level updraft to maintain itself, or at least alter the amount of time taken to re-organize itself after crossing the boundary.

As mentioned in the discussion of Chapter 3, the angle at which the storm crosses the boundary is likely of importance. It would be worthwhile to attempt to adjust the angle the storm crosses the boundary; namely, attempting to have the storm cross at a smaller angle (such that the storm spends more time crossing the boundary) would be interesting, as this could lead to a longer period of time for the storm to acquire additional vorticity along the boundary. Also, a smaller crossing angle may not cut-off the low-level updraft as drastically.

APPENDIX

Appendix A

Trajectory Sensitivity

Since the flows in and around thunderstorms are inherently turbulent, trajectory sensitivity was performed and analyzed to ensure results for both the ascending and descending trajectories are robust. We want to know how small changes in trajectory release time altered the vorticity analysis of the original seed time from Fig. 27. In order to carry out this task, trajectories were seeded and tracked backward in time using the same seeding criteria as discussed in chapter 2. The trajectories were seeded 100 s before and after the original seed time from Fig. 27. Plots were constructed in the same fashion as Figs. 29 and 30, where the average trajectory is shown. Results from both Figs. 29 and 30 and reshown along with the perturbed +/– 100 s averaged trajectories.

Figure 31 (a-h) shows the before crossing average trajectories. In height, vorticity, and vorticity production terms, the trends between each of the trajectories are similar. The same trend similarities are seen in the after crossing case trajectories (Fig. 32a-h). In general, there are no major differences between each of the average trajectories when compared to each other and builds confidence that the rising trajectory results are robust, at least for the storm case presented herein.

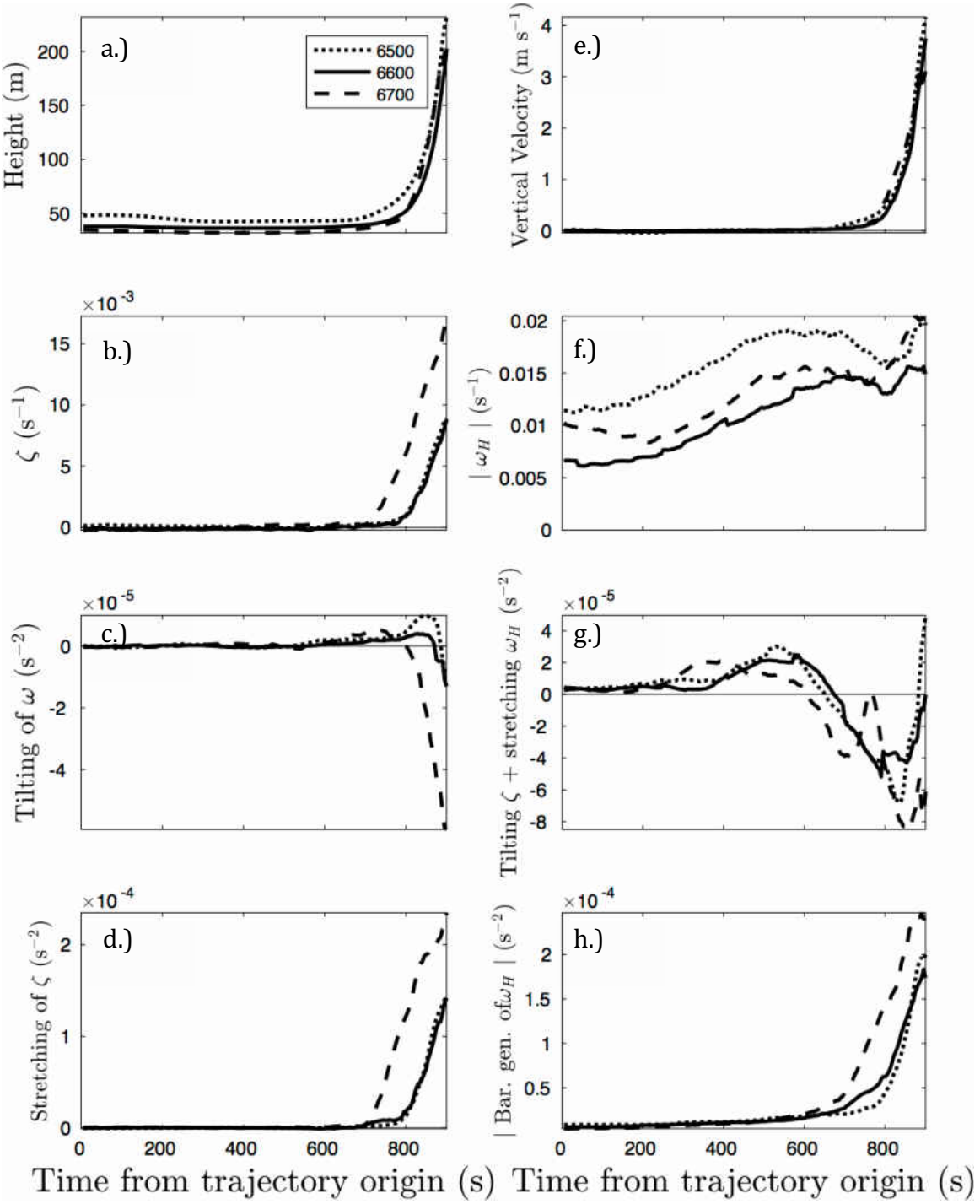

Figure 31. Same as Fig. 29 except showing the three average rising trajectories from the two sensitivity tests in before crossing case. The original rising trajectory (6600 s) is shown for comparison.

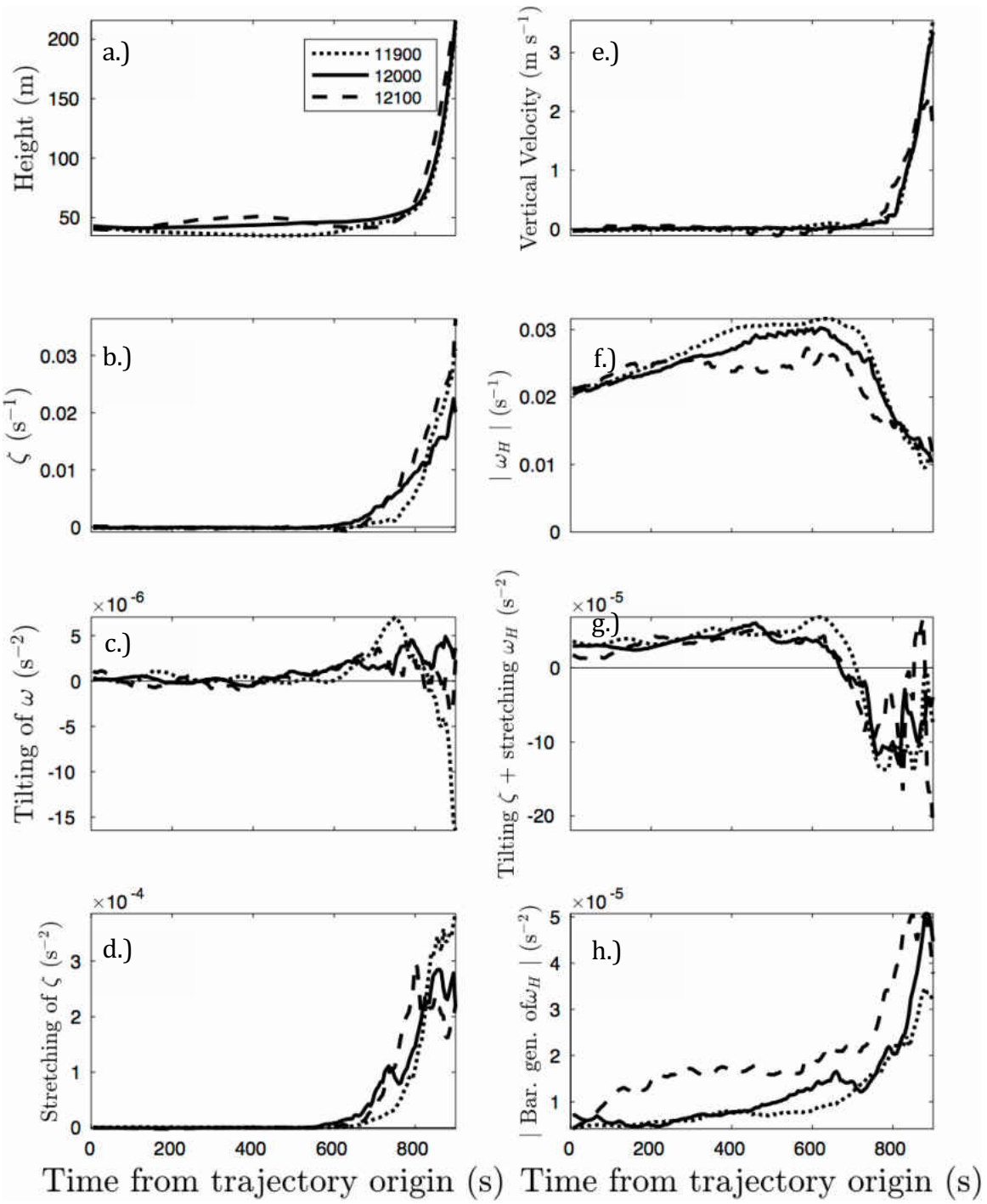

Figure 32. Same as Fig. 29 except showing the three average rising trajectories from the two sensitivity tests in after crossing case. The original rising trajectory (12000 s) is shown for comparison.

Figure 33 (a-h) shows the before crossing descending trajectories. Once again, the general patterns of vorticity and the production terms are similar. All three trajectories have clearly decreasing vertical velocity as they descend "steeply" to the 100 m vertical level. This being an important point in elucidating differences between the before and after crossing descending trajectories from the discussion of how the descending trajectories re-orient the negative vertical vorticity to positive vertical vorticity (see Chapters 3 and 4). The argument that the after crossing trajectories do not have such a "steep" descent toward the 100 m vertical level withstands the sensitivity tests as well (Fig. 34 a,b,c,d,e). Figure 34 (f,g,h) also shows the same general trends from the three separate seeding times.

With the main argument from the conclusions (see end of Chapter 3 or Chapter4) being the different descending slopes from the before and after crossing cases in their importance in how vertical vorticity is generated, these sensitivity tests act to confirm the robustness of the results presented within this study. The rising trajectory sensitivity tests all show close agreement with each other with only minor differences in magnitude shown at times. The reader is reminded that this is not a claim that these sensitivity results are valid for all storm boundary crossing situations. It is likely that the environments on each side of a boundary play a major role in low-level vorticity sensitivity and how vorticity is processed.

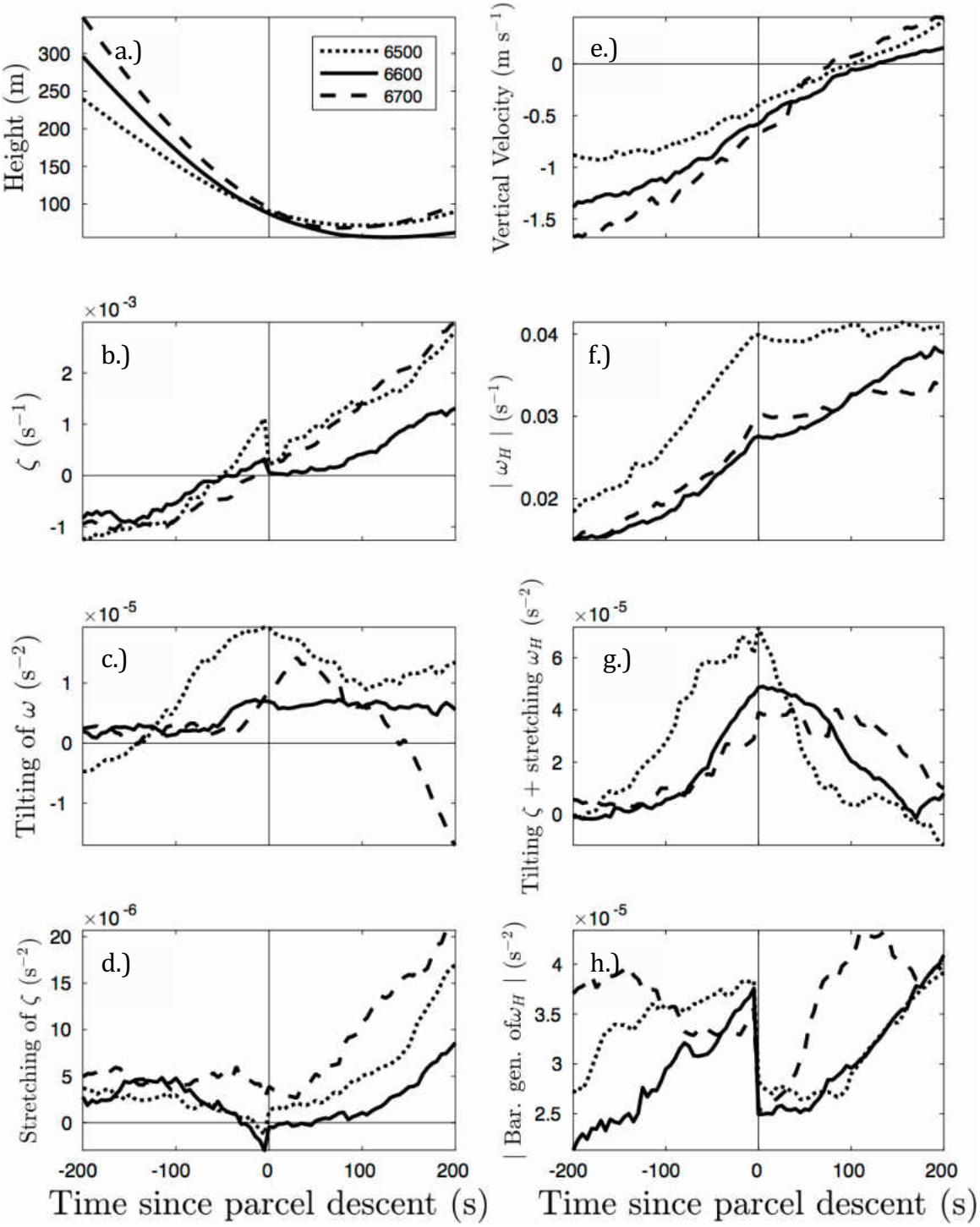

Figure 33. Same as Fig. 30 except showing the two average descending trajectories from the two sensitivity tests in after crossing case. The original rising trajectory (6600 s) is shown for comparison.

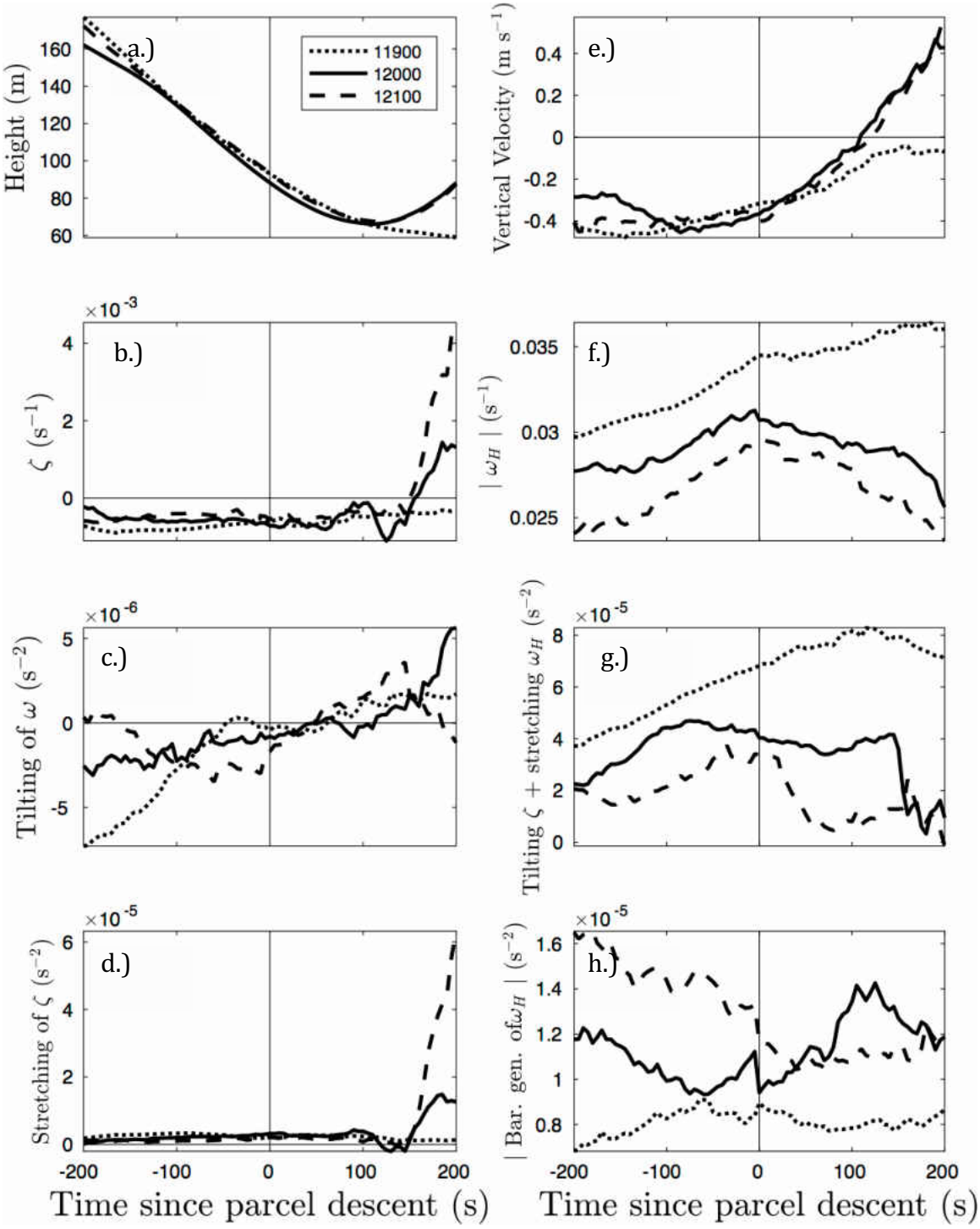

Figure 34. Same as Fig. 30 except showing the two average rising trajectories from the two sensitivity tests in after crossing case. The original rising trajectory (12000 s) is shown for comparison.

REFFERENCES

Atkins, N. T., M. L. Weisman, L. J. Wicker, 1999: The Influence of Preexisting Boundaries on Supercell Evolution. *Mon. Wea. Rev.*, **127**, 2910–2927.

Blanchard, D. O., 2008: Interactions between a Supercell and a Quasi-Stationary Frontal Boundary. *Mon. Wea. Rev.*, **136**, 5199–5210.

Brandes, E. A., & Brandes, E. A. (1984). Relationships Between Radar-Derived Thermodynamic Variables and Tornadogenesis. *Http://Dx.Doi.org/10.1175/1520-0493(1984)1122.0.CO;2*, *112*(5), 1033–1052.

Brooks, H. E., C. A. Doswell III, and R. Davies-Jones, 1993: Environmental helicity and the maintenance and evolution of lowlevel mesocyclones. *The Tornado: Its Structure, Dynamics, Prediction and Hazards, Geophys. Monogr.,* No. 79, Amer. Geophys. Union, 97–105

Bryan, G. H., Fritsch, J. M., Bryan, G. H., & Fritsch, J. M. (2002). A Benchmark Simulation for Moist Nonhydrostatic Numerical Models. *Http://Dx.Doi.org/10.1175/1520-0493(2002)1302.0.CO;2*, *130*(12), 2917–2928.

Bryan, G. H., Wyngaard, J. C., Fritsch, J. M., & Wyngaard, J. C. (2003). Resolution Requirements for the Simulation of Deep Moist Convection. *Http://Dx.Doi.org/10.1175/1520-0493(2003)1312.0.CO;2*, *131*(10), 2394–2416.

Bunkers, M. J., Hjelmfelt, M. R., Smith, P. L., Bunkers, M. J., Hjelmfelt, M. R., & Smith, P. L. (2006). An Observational Examination of Long-Lived Supercells. Part I: Characteristics, Evolution, and Demise. *Dx.Doi.org*, *21*(5), 673–688.

Dahl, J. M. L., M. D. Parker, and L. J. Wicker, 2012: Uncertainties in trajectory calculations within near-surface mesocyclones of simulated supercells. Mon. Wea. Rev., 140, 2959–2966.

Davenport, C. E., Parker, M. D., Davenport, C. E., & Parker, M. D. (2015). Impact of Environmental Heterogeneity on the Dynamics of a Dissipating Supercell Thunderstorm. *Dx.Doi.org*, *143*(10), 4244–4277.

Droegemeier, K. K., & Wilhelmson, R. B. (1987). Numerical Simulation of Thunderstorm Outflow Dynamics. Part I: Outflow Sensitivity Experiments and Turbulence Dynamics. *Http://Dx.Doi.org/10.1175/1520-0469(1987)0442.0.CO;2*, *44*(8), 1180–1210.

Fierro, A. O., Gilmore, M. S., Mansell, E. R., Wicker, L. J., Straka, J. M., Fierro, A. O., & Mansell, E. R. (2006). Electrification and Lightning in an Idealized Boundary-Crossing Supercell Simulation of 2 June 1995*.

Gilmore, M. S., & Wicker, L. J. (2002). Influences of the Local Environment on Supercell Cloud-to-Ground Lightning, Radar Characteristics, and Severe Weather on 2 June 1995*. *Monthly Weather Review*, *130*(10), 2349–2372.

Gilmore, M.S., Wicker, L. J., Mansell,E.R., Straka,J.M., & Rasmussen,E.N., (2002). IDEALIZED BOUNDARY-CROSSING SUPERCELL SIMULATIONS OF 2 JUNE 1995. Conference Preprint. 21st Conference on Severe Local Storms, San Antonio, TX, 12-16 August 2002.

Klemp, J. B., Wilhelmson, R. B., & Wilhelmson, R. B. (1978). The Simulation of Three-Dimensional Convective Storm Dynamics. *Http://Dx.Doi.org/10.1175/1520-0469(1978)0352.0.CO;2*, *35*(6), 1070–1096.

Klemp, J. B., and R. Rotunno, 1983: A study of the tornadic region within a supercell thunderstorm. *J. Atmos. Sci.,* **40,** 359–377.

Klemp, J. B. (1987). Dynamics of Tornadic Thunderstorms. *Annu. Rev. Fluid Mech.*, *19*(1), 369–402. http://doi.org/10.1146/annurev.fl.19.010187.002101

Kuhn, P. M., G. L. Darkow, and V. E. Suomi, 1958: A mesoscale investigation of pre-tornado thermal environments. *Bull. Amer. Meteor. Soc.,* **39,** 224–228.

Lemon, L.R., C. A. Doswell, 1979: Severe thunderstorm evolution and mesocyclone structure as related to tornadogenesis. *Mon. Wea. Rev.*, **107**, 1184–1197

Letkewicz, C. E., French, A. J., Parker, M. D., Letkewicz, C. E., & French, A. J. (2013). Base-State Substitution: An Idealized Modeling Technique for Approximating Environmental Variability. *Dx.Doi.org*, *141*(9), 3062–3086.

Maddox, R. A., L. R. Hoxit, and C. F. Chappell, 1980: A study of tornadic thunderstorm interactions with thermal boundaries. *Mon. Wea. Rev.,* **108,** 322–336.

Magor, B. W., 1959: Mesoanalysis: Some operational analysis techniques utilized in tornado forecasting. *Bull. Amer. Meteor. Soc.,* **40,** 499–511.

Markowski, P. M, E. N. Rasmussen, and J. M. Straka, 1998: The occurrence of tornadoes in supercells interacting with boundaries during VORTEX-95. *Wea. Forecasting,* **13,** 852–859.

Markowski, P. M., Rasmussen, E. N., Straka, J. M., Dowell, D. C., & Dowell, D. C. (1998). Observations of Low-Level Baroclinity Generated by Anvil Shadows. *Http://Dx.Doi.org/10.1175/1520-0493(1998)1262.0.CO;2*, *126*(11), 2942–2958.

Miller, R. C., 1967: Notes on analysis and severe-storm forecasting procedures of the Military Weather Warning Center. Tech. Rep. 200, U.S. Air Force Air Weather Service, 170 pp.

Moller, A. R., C. A. Doswell, M. P. Foster, G. R. Woodall, 1994: The Operational Recognition of Supercell Thunderstorm Environments and Storm Structures. *Wea. Forecasting*, **9**, 327–347.

Naylor, J., and M.S. Gilmore, 2012b: Environmental factors influential to the duration and intensity of tornadoes in simulated supercells. Geophys. Res. Lett., 39, L17802

Naylor, J., and Gilmore, M. S.,(2014). Vorticity Evolution Leading to Tornadogenesis and Tornadogenesis Failure in Simulated Supercells. *Dx.Doi.org*, *71*(3), 1201–1217. http://doi.org/10.1175/JAS-D-13-0219.1

Purdom, J. F. W., 1993: Satellite observations of tornadic thunderstorms. *The Tornado: Its Structure, Dynamics, Prediction and Hazards, Geophys. Monogr.,* No. 79, Amer. Geophys. Union, 265–274.

Rasmussen, E. N., J. M. Straka, R. Davies-Jones, C. A. Doswell III, F. H. Carr, M. D. Eilts, and D. R. MacGorman, 1994: Verification of the Origins of Rotation in Tornadoes Experiment: VORTEX. *Bull. Amer. Meteor. Soc.,* **75,** 995–1006.

Rasmussen, E. N., Richardson, S., Straka, J. M., Markowski, P. M., Blanchard, D. O., Richardson, S., et al. (2000). The Association of Significant Tornadoes with a Baroclinic Boundary on 2 June 1995. *Http://Dx.Doi.org/10.1175/1520-0493(2000)1282.0.CO;2*, *128*(1), 174–191.

Rasmussen, E. N., Rutledge, S. A., & Rutledge, S. A. (1993). Evolution of Quasi-Two-Dimensional Squall Lines. Part I: Kinematic and Reflectivity Structure. *Http://Dx.Doi.org/10.1175/1520-0469(1993)0502.0.CO;2*, *50*(16), 2584–2606.

Richardson, Y. P., Droegemeier, K. K., Davies-Jones, R. P., Richardson, Y. P., Droegemeier, K. K., & Davies-Jones, R. P. (2007). The Influence of Horizontal Environmental Variability on Numerically Simulated Convective Storms. Part I: Variations in Vertical Shear.

Rotunno, R. (1981). On the Evolution of Thunderstorm Rotation. *Http://Dx.Doi.org/10.1175/1520-0493(1981)1092.0.CO;2*, *109*(3), 577–586.

Rotunno, R., & Klemp, J. (1985). On the Rotation and Propagation of Simulated Supercell Thunderstorms. *Http://Dx.Doi.org/10.1175/1520-0469(1985)0422.0.CO;2*, *42*(3), 271–292.

Rotunno,R.,J.B. Klemp , and M. L. Weisman, 1988: A theory for strong, longlived squall-lines. *J. Atmos. Sci.,* **45,** 463–485.

Thompson, R. L., R. Edwards, J. A. Hart, K. L. Elmore, and P. M. Markowski (2003), Close proximity soundings within supercell environments obtained from the rapid update cycle, Weather Forecast., 18, 1243–1261

Weaver, J. F., and S. P. Nelson, 1982: Multiscale aspects of thunderstorm gust fronts and their effects on subsequent storm development. *Mon. Wea. Rev.,* **110,** 707–718.

Weaver, J.F., J.F.W. Purdom, and E. J. Szoke, 1994: Some mesoscale aspects of the 6 June 1990 Limon, Colorado, tornado case. *Wea. Forecasting,* **9,** 45–61.

Weaver, J.F., J.F.W. Purdom, and E. J. Szoke, 1994: Some mesoscale aspects of the 6 June 1990 Limon, Colorado, tornado case. *Wea. Forecasting,* **9,** 45–61.

Weisman, M. L., and J. B. Klemp, 1982: The dependence of numerically simulated convective storms on vertical wind shear
and buoyancy. *Mon. Wea. Rev.,* **110,** 504–520.